



The Ionosphere of Mars After 20 Years of Mars Express Contributions

Kerstin Peter¹ · Beatriz Sánchez-Cano² · František Němec³ · Francisco González-Galindo⁴ · Andrew J. Kopf⁵ · Mark Lester² · Martin Pätzold¹ · Catherine E. Regan⁶ · Mats Holmström⁷

Received: 31 July 2023 / Accepted: 8 May 2024 / Published online: 28 May 2024
© The Author(s) 2024

Abstract

The Martian ionosphere originates from the ionization of the planetary neutral atmosphere by solar radiation. This conductive layer is embedded within the thermosphere and exosphere of Mars where it forms a highly variable interaction region with the solar wind. The Martian ionosphere has been continuously observed by the three plasma instruments MaRS, MARSIS and ASPERA-3 on Mars Express for the last 20 years (> 10 Martian years). Those long-term observations laid a solid foundation for what we know today about the Martian ionosphere, and provided numerous opportunities for collaboration and coordinated observations with other missions. This review describes the most significant achievements of Mars Express for the ionosphere, such as the dynamics and structures of both day and night-side, its variability and couplings with the lower atmosphere, as well as the improvement of atmospheric and ionosphere modelling. Mars Express has also provided a better characterization of the role of several external and internal drivers in controlling the ionosphere, such as the Martian crustal magnetic fields, solar activity, seasons, dust lifting from the surface, and even the direct interaction of the Martian ionosphere with the coma of an Oort-cloud comet (C/2013 A1, Siding Spring).

Keywords Mars Express · Mars · Ionosphere

1 Introduction

The ionosphere of a planet is defined as the part of its atmosphere where free ions and electrons are present in a significant amount. At Mars, the ionosphere is found between approximately 80 and 400 km altitude. It includes parts of the planetary mesosphere, thermosphere and exosphere, but less than 1‰ of the neutral atmosphere at the ionospheric main peak is ionized. The dominant ion at the ionospheric main peak is O₂⁺, which originates from the photoionization of CO₂ and subsequent rapid reactions. Mars has no detectable global intrinsic magnetic field. The solar wind therefore interacts directly with the extended planetary atmosphere and ionosphere to form a magnetic barrier that can deflect the solar wind around Mars. Crustal magnetic anomalies, which are strongest on a particular region of the southern hemisphere, complicate the Mars-solar wind interaction, as these fields have the

Extended author information available on the last page of the article

capacity to reconnect with the interplanetary magnetic field of the solar wind creating a hybrid interaction over that region, with features of an induced and intrinsic magnetosphere (Xu et al. 2017).

The Mars Express (MEX) spacecraft (Chicarro et al. 2004) has been in orbit around Mars since December 2003 and is still healthy after more than 20 years. Observations extend from solar cycle 23 to 25 and cover more than 10 full Martian years. Mars Express is equipped with three plasma experiments to support ionospheric investigations: i.) Mars Radio Science (MaRS) (Pätzold et al. 2004, 2009) observes the Mars atmosphere during two-way Earth occultations in either single X-Band (~ 8.4 GHz), S-Band (~ 2.1 GHz) or coherent dual-frequency mode and provides profiles¹ of the ionospheric electron density and the temperature, pressure and particle density of the lower neutral atmosphere, ii.) the Mars Advanced Radar for Subsurface and Ionosphere Sounding (MARSIS), which has two operational modes from which ionospheric observations can be retrieved (the Active Ionospheric Sounding, AIS, and the Subsurface mode) (Picardi et al. 2004; Orosei et al. 2015), and iii.) the Analyzer of Space Plasma and Energetic Atoms (ASPERA-3) sensor package to investigate the interaction of the solar wind with Mars (Barabash et al. 2004). General descriptions of the individual instruments can be found in Wilson et al. (2024), this collection. This article summarizes the highlights of the discoveries made by Mars Express and illustrates how the mission has significantly contributed to our knowledge about the Mars' plasma system. More than 20 years of Mars Express observations provide a solid base for ionospheric investigations and pushed the boundaries of our current knowledge about the Mars ionosphere, in particular about its formation and variability, the coupling with the lower atmosphere, its role as a protective boundary to the solar wind and its impact on planetary evolution.

2 Observation Conditions for Mars Year 27 to 36

Primary drivers for the formation and variability of Mars' ionosphere are variations in the Sun's output (solar cycle, solar wind, irradiance), variations in Mars orbital (perihelion/aphelion) and obliquity (summer/winter) seasons and the individual and combined effects of those factors on the Mars neutral atmosphere and surface. Figure 1b illustrates the variation of the integrated solar irradiance up to the FUV (≤ 190 nm, Φ_{190}) at Mars. The dominant factor for changes in Φ_{190} (and even more for the total solar irradiance) at the Mars position is not the solar cycle, but the change in Mars-Sun distance from Mars aphelion to perihelion (Fig. 1a, b). The large orbit eccentricity of Mars of 0.09 leads to an increase in total insolation from Mars aphelion (solar longitude $L_S=71^\circ$) to perihelion ($L_S=251^\circ$) by approx. 45%. Stronger solar cycle effects are seen in the solar EUV (Fig. 1c) and solar X-ray radiation (Fig. 1d). The summer solstice of the southern hemisphere occurs when the path of the subsolar point on the planetary surface reaches its farthest southern extension. At Mars, the southern summer solstice occurs in close alignment with Mars perihelion. Therefore, the orbital seasons and obliquity seasons align on the southern hemisphere and disalign on the northern hemisphere. This results in higher insolation on the southern hemisphere during southern summer than on the northern hemisphere during northern summer, which strongly affects the Mars dust cycle.

¹The deviation of a radio science observation from a strictly vertical altitude profile depends on the orbit geometry and the time the occultation observation occurs along the orbit. The median change of the projected footpoint location on the planetary surface during an observation is 2.0° in longitude and 2.9° in latitude between 50 and 400 km altitude in the current MaRS dataset.

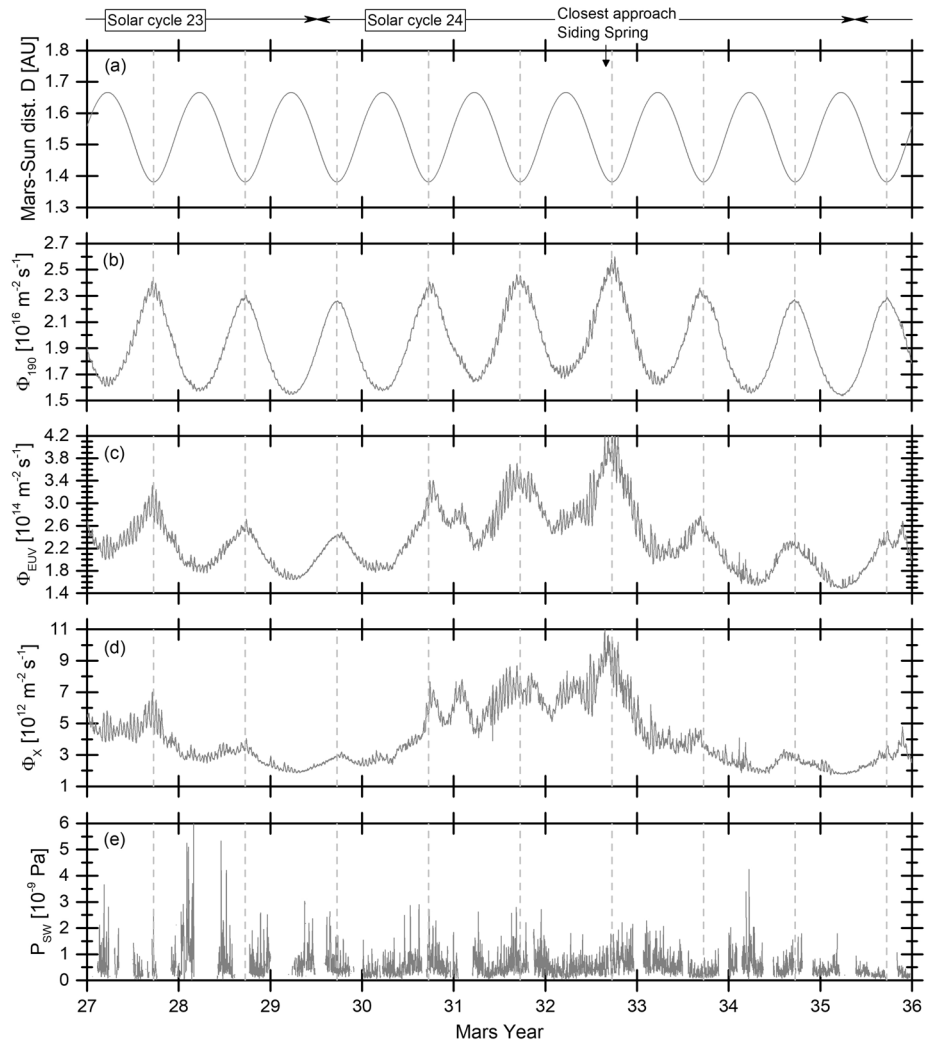


Fig. 1 Variation of selected environmental parameters during the MEX mission: (a) Mars-Sun distance D . The integrated solar radiation at the Mars position is shown in (b) $\Phi_{190} \leq 190$ which includes solar radiation up to the Far UltraViolet (FUV) which affects the heating of the thermosphere and hence the scale height of the ionosphere, (c) $10 \text{ nm} \leq \Phi_{EUV} \leq 95 \text{ nm}$ as proxy for the solar Extreme UltraViolet (EUV) and (d) $\Phi_X < 10 \text{ nm}$ as proxy for solar X-ray. The solar radiation is derived from the MAVEN LPW-EUVM based FISM-M model (Thiemann et al. 2017) and FISM V2 (Chamberlin et al. 2020) solar radiation data for Earth (details in Peter et al. 2023). (e) 1-day average solar wind dynamic pressure based on MEX ASPERA-3 observations (Ramstad et al. 2015). The vertical dashed lines indicate Mars perihelion. The arrow indicates the closest encounter between Mars and the comet Siding Spring on 19 October 2014

Dust aerosols are an effective driver for the variability of the Mars neutral atmosphere and ionosphere. The dust cycle on Mars can be roughly divided into two seasons (see also Määttänen et al. 2024, this collection). In the non-dusty season (approximately $L_S=0^\circ$ to $L_S=135^\circ$) the dust load of the atmosphere is generally low. The dust load increases during the dusty season (approximately $L_S=135^\circ$ to $L_S=360^\circ$, e.g. Kahre et al. 2017), where

the largest dust events are observed (Wang and Richardson 2015). Large-scale dust storms, where the whole planet is engulfed in dust, occur at irregular intervals on Mars. Two big planet-encircling dust events (PEDEs) occurred during the mission time of MEX, in Mars Year 28 and in Mars Year 34.

In addition to these sources for ionospheric variability, the Martian environment is strongly affected by the solar wind (Fig. 1e) and by short and intense space weather events. Solar flares (Futaana et al. 2008) and solar energetic particles (SEPs) (Sánchez-Cano et al. 2019) interact with the lower ionosphere of Mars. Coronal mass ejections (CMEs) (Kajdič et al. 2021) or Stream Interaction Regions (SIRs) cause solar wind dynamic pulses and transients in the solar wind which can compress the topside ionosphere. Mars Express observations provide the basis for pioneering research in this field by showing that all of the previously mentioned solar events enhance the dynamics of the ionosphere of Mars on different time scales and that the intensity of those interactions strongly depends on the solar cycle (details in Sect. 5).

Of special interest was the close encounter with the Oort-cloud comet C/2013 A1 (Siding Spring) and Mars in October 2014, which provided an unique opportunity for Mars Express to investigate the interaction between a cometary environment and a planetary atmosphere.

3 The Dayside Ionosphere

Photochemical processes dominate the formation of the main ionospheric region on the planetary dayside of Mars up to approximately 200 km altitude. Above this altitude, plasma transport processes become dominant (Fig. 2a). The two main features of the undisturbed dayside ionosphere are the ionospheric main peak M2² and the weaker secondary region M1 below (Fig. 2). The main source for the formation of the M2 region is photoionization by solar EUV, while the lower region M1 is created from the primary photoionization and secondary electron impact ionization by solar X-ray < 10 nm (Fox et al. 1996). The ratio of secondary electron impact ionization to primary photoionization is known as the ionization efficiency, which ranges from 0.1 - 0.3 (depending on SZA and season) above neutral pressures of $1 \cdot 10^{-6}$ Pa down to > 100 near $1 \cdot 10^{-3}$ Pa (Lillis et al. 2021b). While the M2 region on the ionospheric dayside regularly occurs as a pronounced peak, the M1 feature appears as a smooth shoulder. M1 regions with clear peaks regularly occur only in observations with large observational noise, indicating either a disturbed ionosphere or observational bias as a source for the peak in the observations. Below the M1 region Pätzold et al. (2005) discovered transient accumulations of electron density in MaRS observations (Fig. 7b, c), which were originally attributed to the ablation and ionization of meteoric material (e.g. Whalley and Plane 2010). A solely meteoric origin of the accumulations is, however, unlikely (see Crismani et al. 2017; Peter 2018; Peter et al. 2021 and Sect. 5 of this publication). Sporadically, intense ionospheric layers mainly composed of O₂⁺ are found globally between 50 and 100 km caused by particle precipitation, particularly after showers of solar energetic particles (Sánchez-Cano et al. 2019; Nakamura et al. 2022).

A transient feature in the topside ionosphere of Mars, which was also unknown prior to the arrival of Mars Express, is regularly observed by MARSIS (Kopf et al. 2008, 2017) (Fig. 2d, e) and also in Mars Global Surveyor (Mayyasi et al. 2018), MAVEN ROSE (Mukundan et al. 2022) and MEX MaRS (Peter et al. 2022) radio science observations

²Notation after Rishbeth and Mendillo (2004). Other terms include F1 and E for M2 and M1 to indicate formation process comparable to the Earth ionosphere (e.g. Bauer and Hantsch 1989, Fox and Yeager 2006).

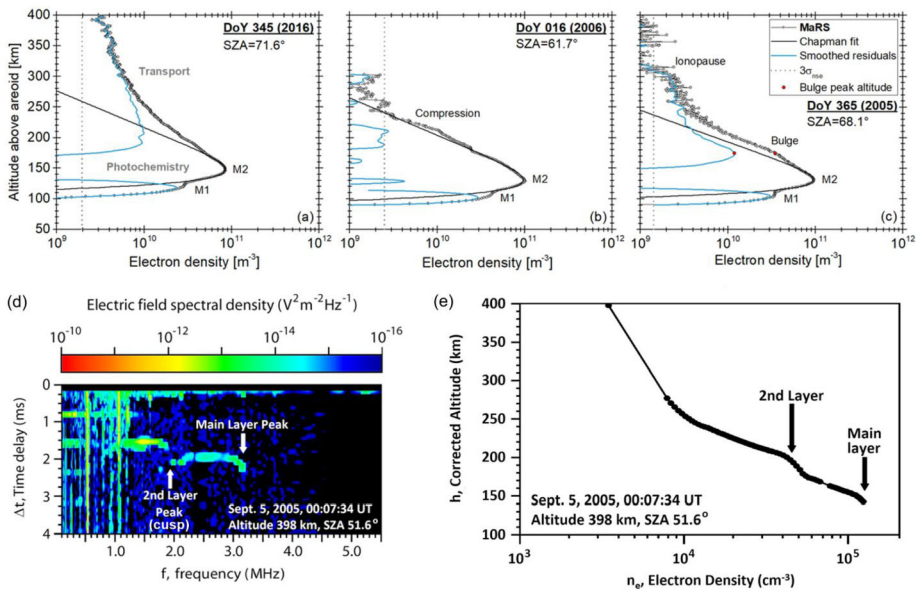


Fig. 2 Panel (a) to (c) contain MaRS radio science observations of the Mars dayside ionosphere. Gray circles show the derived electron density, while the gray dashed line indicates the noise level of the observation $3 \cdot \sigma_{N_{se}}$. The black line is the result of a Chapman function fit on the ionospheric main peak region, while the blue line indicates the smoothed residuals of the fit. The red dot indicates the identified bulge in observation and residuals (details in Peter et al. 2014, 2023). (d) MARSIS ionogram containing a geometric cusp at lower frequencies, which is the characteristic signature of a second topside layer. (e) Corresponding electron density profile (from Fig. 1 of Kopf et al. 2017)

(Fig. 2c, Fig. 7b). Terms used in the literature for the transient accumulations of electron density in the topside ionosphere include bulge, second layer or M3. Potential origins of this feature will be discussed in Sect. 5.

The upper region of the Mars dayside ionosphere is dominated by transport processes. The extent and shape of this region is highly variable on temporal scales and ranges from approximately exponential decay (Fig. 2a) to strongly compressed shapes (Fig. 2b). The interaction of Mars with the solar wind is that of an unmagnetized planet like Venus, except for the inhomogeneous and locally-strong crustal magnetic fields, concentrated in the southern hemisphere and rotating with the planet (Connerney et al. 2001). MARSIS and MaRS (Fig. 2c) both observe ionopause-like structures at Mars for the very first time, whose origin will be discussed in detail in Sect. 5.

Before the arrival of Mars Express, regular observations of the dayside ionosphere with Mars Global Surveyor were constrained to solar zenith angles between 70° and 90°. MaRS extended this range to 50° > SZA > 130° and confirmed that the solar zenith angle dependence of the ionospheric main peak electron density (Fig. 3c) and Total Electron Content (TEC, integrated vertical electron content of an ionospheric profile, Fig. 3a) extends to lower SZAs. The dayside TEC as well as the M2 peak electron density show a strong correlation with the solar EUV irradiation available at the Mars position. For the first time, MaRS observations showed a similar correlation between the M1 TEC/peak electron density (Fig. 3b, d) and the SZA in combination with solar X-ray (0-10 nm) (Pätzold et al. 2009; Peter et al. 2014, 2021) irradiation. The M2 and M1 dayside ionospheric peak altitudes are affected by the SZA of the observation as well as by the Mars-Sun distance (Fig. 4). The increase in

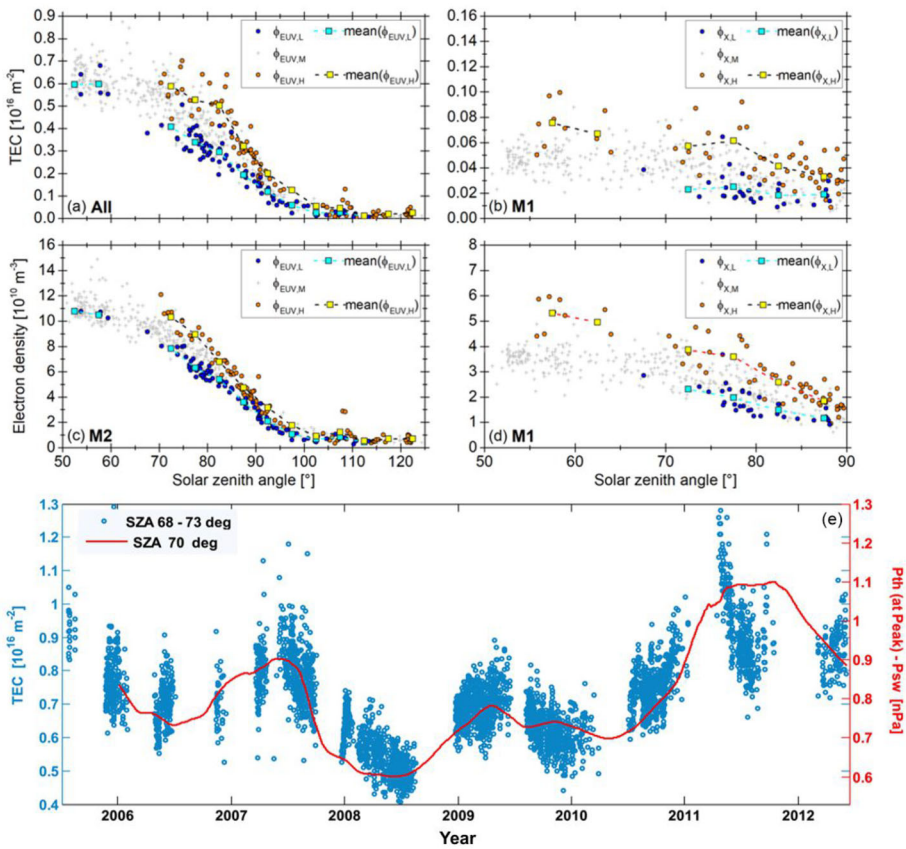


Fig. 3 Mars ionosphere (a) Total Electron Content (TEC), (b) M1 TEC, (c) M2 peak electron density and (d) M1 electron density as function of SZA. TEC and M2 peak electron density are distinguished by low ($\Phi_{EUV,L} < 1.9 \cdot 10^{14} \text{ s}^{-1} \text{ m}^{-2}$), moderate ($1.9 \cdot 10^{14} \text{ s}^{-1} \text{ m}^{-2} \leq \Phi_{EUV,M} \leq 2.7 \cdot 10^{14} \text{ s}^{-1} \text{ m}^{-2}$) and high ($\Phi_{EUV,H} > 2.7 \cdot 10^{14} \text{ s}^{-1} \text{ m}^{-2}$) integrated solar EUV (10-95 nm) fluxes, M1 TEC and M1 peak electron density by integrated solar X-ray (0-10 nm) with $\Phi_{X,L} < 2.3 \cdot 10^{12} \text{ s}^{-1} \text{ m}^{-2}$, $2.3 \cdot 10^{12} \text{ s}^{-1} \text{ m}^{-2} \leq \Phi_{X,M} \leq 5.3 \cdot 10^{12} \text{ s}^{-1} \text{ m}^{-2}$, $\Phi_{X,H} > 5.3 \cdot 10^{12} \text{ s}^{-1} \text{ m}^{-2}$. Averages are calculated for 5° SZA bins (updated Fig. 5 of Peter et al. 2023). (e) Variation of MARSIS subsurface TEC with the solar cycle. The red line indicates the pressure difference between the maximum thermal pressure from MARSIS AIS mode and the solar wind dynamic pressure (Fig. 10 of Sánchez-Cano et al. 2016)

insolation from aphelion to perihelion in combination with Mars’ dust cycle causes a rise of the M2 and M1 dayside peak altitudes (Peter et al. 2023, Fig. 17d).

The exceptional temporal and spatial coverage of MARSIS provides information about the ionospheric topside for all SZA. The derived ionospheric peak densities were used to study the Martian ionosphere under changing observation conditions (Morgan et al. 2008). It was shown that the scale height of the ionospheric transport region is controlled by the induced magnetic fields (Němec et al. 2011b) and by the solar cycle variation (Sánchez-Cano et al. 2015, 2016). MARSIS provided the first TEC observation over the whole ionospheric dayside (Lillis et al. 2010), over the Martian polar caps (Sánchez-Cano et al. 2018) and continuous observations over a whole solar cycle (Sánchez-Cano et al. 2016) (Fig. 3e). During periods of low ionizing solar flux at Mars, MARSIS observed the lowest levels of ionization

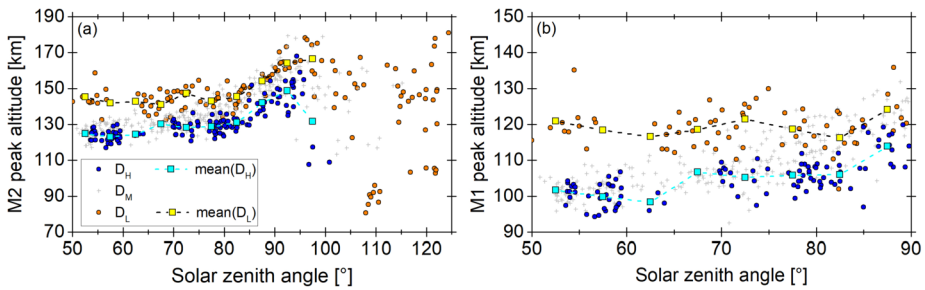


Fig. 4 Mars ionospheric peak altitude M2 (a) and M1 peak altitude (b) as a function of SZA and distinguished by low (D_L), moderate (D_M) and high (D_H) Mars-Sun distances. Averages are calculated for 5° SZA bins (updated Fig. 6 of Peter et al. 2023)

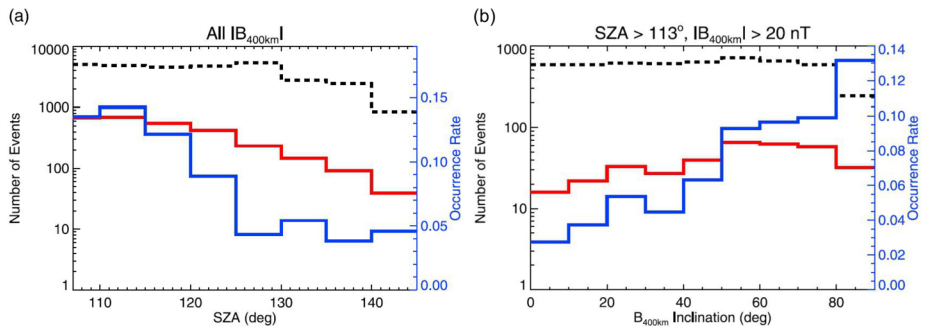


Fig. 5 Detections of the nightside ionosphere in MARSIS subsurface TEC observations as a function of SZA. The black dashed line represents the total number of observations per SZA. The red line indicates the number of successful detections, while the blue line gives the percentage of successful detections (right scale). (a) all data, (b) magnitudes of the magnetic field > 20 nT in 400 km altitude (Fig. 3 of Němec et al. 2010)

ever seen by a Mars mission, an irradiation effect which is also seen in the Earth ionosphere (Sánchez-Cano et al. 2015). This behavior has been recently corroborated when the long lifetime of the MEX mission time allowed the comparison of TEC variability during two consecutive solar minima (2008-2009 and 2018-2020) (Sánchez-Cano et al. 2021b).

4 The Nightside Ionosphere

The terminator is the boundary between the planetary dayside and nightside, with its exact location depending on the investigated physical phenomenon. While the optical terminator (where Mars is optically shadowed from direct solar radiation) increases with increasing solar zenith angle from the surface at 90° SZA to ~ 120 km at 105° SZA, the UV terminator (relevant for the direct ionization of the atmosphere) was found on average 123 km above the optical terminator over one Mars year (Steckiewicz et al. 2019). Two main sources have been suggested as origin for the nightside ionosphere behind the EUV terminator: i.) impact ionization from precipitating particles of either solar wind or dayside photoelectron origin and ii.) day-to night plasma transport driven either by winds or by the planetary rotation of long-lived ions to the nightside (see e.g. summary of Girazian et al. 2017b and references therein).

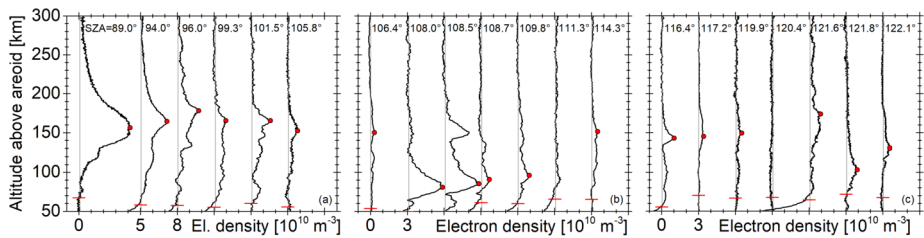


Fig. 6 20 MaRS terminator/nightside electron density profiles observed between August and September 2005. The second profile in (a) has an offset of $5 \cdot 10^{10} \text{ m}^{-3}$, while all other profiles have an offset of $3 \cdot 10^{10} \text{ m}^{-3}$ to the neighbouring profiles. The vertical gray line indicates zero electron density for each profile, the red dot indicates the identified M2 peak electron density (valid if $n_{M2} > 6 \cdot \sigma_{nse}$) and the vertical red line indicates the lowest valid altitude h_L . Based on Fig. 3 of Withers et al. (2012b)

Before the arrival of Mars Express, only sparse information was available about the night-side ionosphere from radio occultations conducted by Mars 4 and 5 in 1974 and the Viking orbiters 1 and 2 during the solar minimum phase in 1977. After the deployment of the MARSIS radar booms in 2005, Safaenili et al. (2007) reported higher electron peak densities above locations where the Martian crustal magnetic fields were closer to vertical than horizontal based on MARSIS Subsurface mode data of the Martian nightside. This irregularity and correlation with crustal fields piqued further interest in the Martian nightside and caused further theoretical and MGS-based studies (see e.g. Lillis and Brain 2013 and references therein).

Peak electron densities in the nightside ionosphere of Mars are usually below the MARSIS detection limit (about 10^{10} m^{-3}). Therefore an ionospheric reflection on the nightside means that the peak electron density is (much) higher compared to regular observation conditions. The occurrence rate of nightside ionospheric reflections in MARSIS observations decreases with SZA up to about 125° , indicating the crucial role of the plasma transport from the dayside as support for the nightside ionosphere (Fig. 5). In regions with strong crustal magnetic fields at higher SZAs, the ionosphere occurrence rate is controlled by the inclination of crustal magnetic fields, indicating the importance of electron impact ionization (Němec et al. 2010, 2011a).

MEX MaRS observations cover SZAs up to 130° and also indicate that the nightside ionosphere is temporally and spatially inhomogeneous (Withers et al. 2012b, Fig. 6). The MaRS data set used for Figs. 3 and 4 contains 91% valid ionospheric peak detections for the planetary nightside. The detections show a continuous decrease in TEC and M2 peak electron density for increasing SZA up to 100° . For higher SZAs the peak electron density usually does not exceed $2 \cdot 10^{10} \text{ m}^{-3}$ (Fig. 3a, c). The ionospheric peak altitude is highly variable on the nightside (Fig. 4a), which is due to the high temporal and spatial variability of the observed ionospheric structures (Fig. 6). Withers et al. (2012b) indicated that the ionospheric peaks present at 90 km altitude can be attributed to SEP events. This finding was confirmed by Harada et al. (2018) who found that a pronounced ionospheric layer with densities up to $\sim 1 - 2 \cdot 10^{10} \text{ m}^{-3}$ was created on the deep nightside (SZA $> 120^\circ$) during a major SEP event in September 2017. This was later corroborated by Sánchez-Cano et al. (2019).

High altitude MARSIS-AIS observations of the Martian tail have shown the motion of cold plasma structures leaving the planet most probably caused by multifactorial transport processes (Stergiopoulou et al. 2020). While the focus of this work is on the results from 20 years of Mars Express observations of the Martian ionosphere, the arrivals of the MAVEN

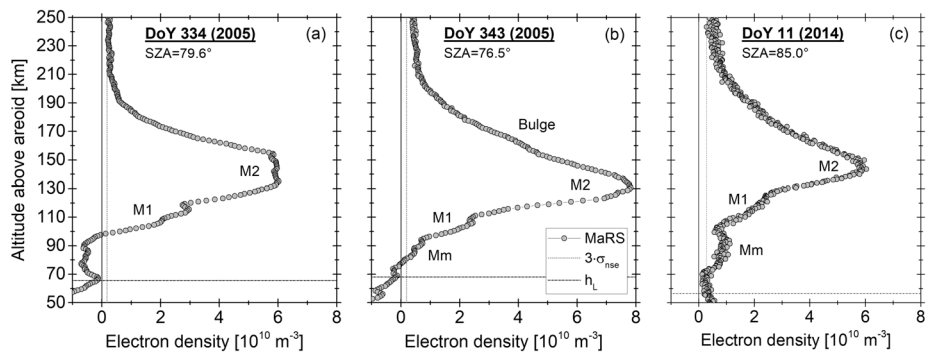


Fig. 7 Three MaRS electron density profiles illustrating atypical features near and below the ionospheric main peak

spacecraft in 2014 and the Emirates Mars Mission (EMM) in 2021 provide new opportunities for completing the picture of the highly complex nightside ionosphere (e.g. Lillis et al. 2018, 2022, Withers et al. 2022, Girazian et al. 2017a, 2023).

5 The Variability of the Mars Ionosphere

5.1 General

The morphology of the Mars ionosphere is remarkably variable and often deviates from the two-layer structure topped by an exponentially decaying transport region seen during a quiet ionosphere (Fig. 2a). Otherwise undisturbed electron density profiles sometimes show deviations from a smooth rounded main peak and display flat-topped (Fig. 7a), sharply pointed or wavy shapes instead (Withers et al. 2012a). The photochemically dominated region of the ionosphere can contain transient accumulations of electron density below the M1 region as well as above the main peak, while the shape and extent of the ionospheric topside varies between a compressed state and exponential decay (Fig. 2), depending on the state of the solar wind. The ionospheric state is locally affected by crustal magnetic fields and globally affected by solar events. The close encounter of Mars with comet Siding Spring during the lifetime of MEX provided a rare opportunity to investigate the direct interaction of a comet with a planetary atmosphere.

5.2 The Lower Ionosphere

The lower base of the Mars dayside ionosphere in MaRS radio science observations (where the observed electron density drops below the noise level beneath M1) is often found between 80 and 90 km altitude. Sporadically, accumulations of electron density are found below the base of the M1 layer (Pätzold et al. 2005) (Fig. 7b, c) and have been first attributed to the ionization of meteoroid dust. A statistical analysis of the MaRS data set between 2004 and 2017 revealed that 42% of the investigated data contains excess electron densities merged (Mm) with the base of M1 in a large variety of shapes (Peter 2018). Mm peak densities are found between approx. $1 \cdot 10^9 \text{ m}^{-3}$ and $1.5 \cdot 10^{10} \text{ m}^{-3}$, where the lower detection limit is provided by the noise level of the radio science observations. Those peak densities make an exclusive origin of the detected Mm by meteoric Mg^+ unlikely, because

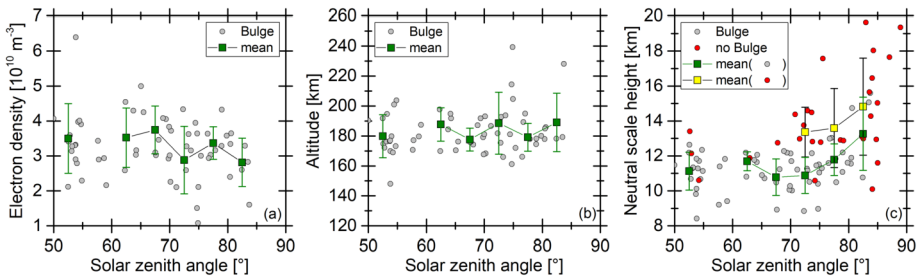


Fig. 8 Bulge characteristics in the undisturbed ionosphere observed by MEX MaRS (feature shown in Fig. 2c). (a) Bulge peak electron densities and (b) altitudes are derived from a quiet and uncompressed subset of 91 MaRS observations ($\sigma_{nse} < 4 \cdot 10^9 \text{ m}^{-3}$, ionosphere exceeds 300 km altitude) (Peter et al. 2022). Green squares and associated error bars indicate the mean and standard deviation of the data in 5° SZA bins. Panel (c) contains the derived neutral scale heights H (determined from the MaRS ionospheric observations by a Chapman function fit) with and without a bulge

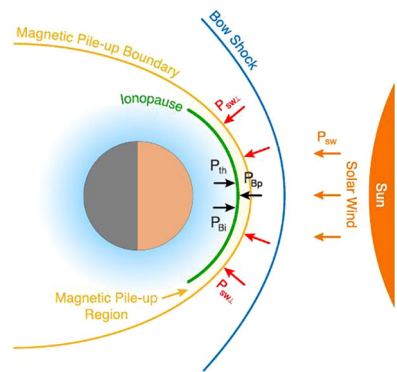
the remote detections of the MAVEN Imaging Ultraviolet Spectrograph between 2014 and 2022 provide only maximum Mg^+ densities of $5 \cdot 10^8 \text{ m}^{-3}$ (observation error of 30%), even during periods of predicted meteor showers or over strong crustal magnetic fields (Crismani et al. 2017, 2023). More likely origins for the identified Mm structures are variations in solar radiation $< 2 \text{ nm}$, local temperature changes during solar flares, particle precipitation, SEPs, gravity waves or deviation from a radial symmetric ionosphere caused by other sources (Peter et al. 2021). The encounter of the Comet C/2013 A1 (Siding Spring) with Mars is discussed in Sect. 5.4.

5.3 The Topside Ionosphere

Transient layers in the topside ionosphere of Mars were not identified in observations prior to the arrival of Mars Express. Kopf et al. (2008, 2017) identified cusps in the MARSIS frequency-time diagrams, which translate into additional distinct ionization layers with local maxima above the main peak (Fig. 2d, e). While a single topside layer is regularly observed at altitudes between about 180 and 240 km, occasionally up to three topside layers were identified in a spectrogram. Transient layers occur more frequently close to the subsolar point (about 60% of the time) and their occurrence decreases down to less than 5% at the terminator. Suggested origins of the transient layers include the dynamic interaction of the solar wind with the upper atmosphere.

MaRS observations of the quiet and uncompressed ionosphere (Fig. 8) indicate that the shape of the undisturbed ionospheric topside varies from a pronounced shoulder shape (bulge in Fig. 2c) to a smooth transition into the ionospheric transport region (Fig. 2a). Only a few of the identified bulges contain weak local electron density maxima (which are identifiable as geometric cusp shapes in the MARSIS ionogram, see Fig. 2d) and no additional pronounced layers between the ionospheric main peak and 250 km altitude were found. This supports the theory of Kopf et al. (2008) that the disturbance of the ionosphere introduced by the solar wind - upper atmosphere interaction is a potential source for the additional topside layers identified in MARSIS observations. As much as 33% of the investigated 91 undisturbed MaRS observations do not contain a detectable bulge. Those profiles are accumulated at higher SZA and show on average a larger neutral scale height than observations with a detectable bulge (Fig. 8c). This implies that the bulge feature in the quiet and uncompressed ionosphere might be merged with the M2 (i.e. main peak) region at higher SZAs

Fig. 9 Individual pressure terms at the ionopause with the ionospheric thermal pressure P_{th} , the magnetic pressure within the ionosphere P_{Bi} , the magnetic pressure in the magnetic pileup region P_{Bp} , and the solar wind dynamic pressure P_{sw} (Figure 1d of Chu et al. 2021)



(Peter et al. 2022). The decrease in probability of a bulge detection for increasing SZA is in good agreement with the findings of MARSIS (Kopf et al. 2008). There is no significant variation in the determined bulge maximum electron density (Fig. 8a) or altitude (Fig. 8b) with SZA. Simulations rule out photoionisation <95 nm as a source for the bulge feature (Peter et al. 2014).

5.4 Ionopause and Pressure Balances Within the Ionosphere

The boundary between the shocked solar wind plasma and the ionosphere of a planet without a global magnetic field is physically described as a tangential discontinuity. The term ionopause was first used for the solar wind boundary with the Venus ionosphere during the Pioneer Venus Orbiter (PVO, 1978-1992) mission. Ionopause definitions for Venus range from the location of pressure balance between the solar wind and the total pressure exerted by the Venusian ionosphere (thermal + magnetic) to the location of a substantial decrease in ion density or electron density within short temporal or spatial scales. In PVO radio science observations the ionopause was identified as that altitude where the electron density passes through $5 \cdot 10^8 \text{ m}^{-3}$ independent of the presence of a gradient. If the thermal pressure of the ionospheric plasma is able to balance the pressure component of the solar wind normal to the interaction surface, the ionosphere remains unmagnetized. Larger solar wind pressures can result in a magnetized ionosphere (see Brace and Kliore 1991 and references therein). The interaction of Mars with the solar wind is that of a globally unmagnetized planet like Venus (Fig. 9), except for the regions with strong crustal magnetic fields (see summary of Sánchez-Cano et al. 2020b and references therein). Gurnett et al. (2010a) used local and remote MARSIS electron density measurements to analyze the characteristics of the solar wind – ionosphere interaction region (Fig. 10). Observed relative density fluctuations increase with altitude and reach a saturation of about 100% at an altitude of about 400 km. The persistent large density fluctuations are consistent with the Kolmogorov spectrum expected from 3D isotropic fluid turbulence in the interaction region, inhibiting the formation of a clear solar wind-ionosphere boundary. The first detection of a steep gradient ionopause at Mars was revealed by Duru et al. (2009) using MARSIS-AIS electron density observations (both local plasma oscillations and remote radar sounding). Those findings were later corroborated by Chu et al. (2019, 2021) and Duru et al. (2020) with larger MARSIS-AIS data sets. In remote radar soundings, a typical Venus-type ionopause was identified in 9% of the observations with an average altitude of 363 ± 65 km and an average thickness of ~ 5.8 ion gyroradii (Chu et al. 2019). In-situ ionopause detections from MARSIS plasma oscillations provided altitudes

Fig. 10 (a) Standard deviation of the electron density observed by MARSIS Δn_e as a function of altitude, (b) $\Delta n_e/n_e$ as a function of altitude. Data above 275 km are from local measurements, data below are from remote sounding measurements. The dashed lines are interpolations between the two types of measurements (Fig. 12 of Gurnett et al. 2010a)

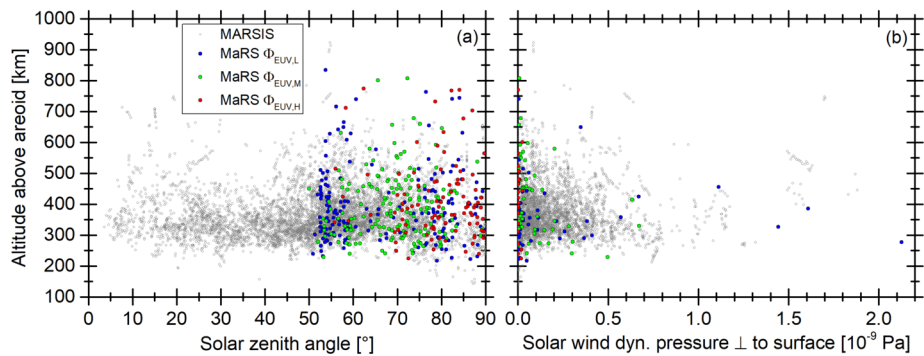
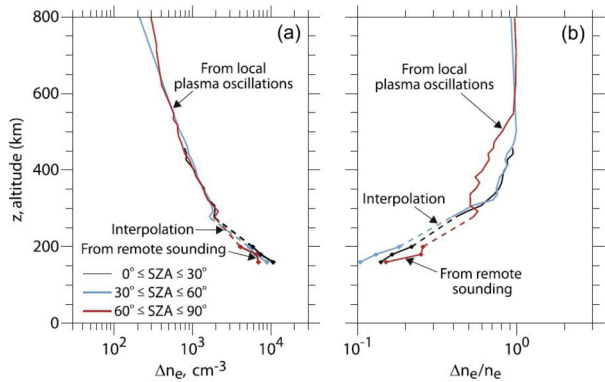
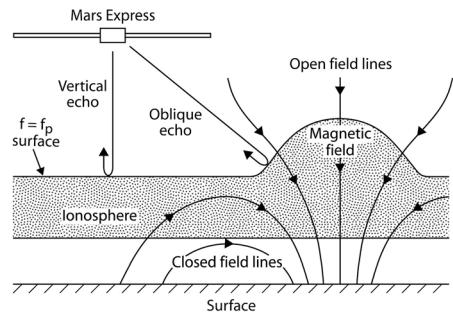


Fig. 11 MARSIS ionopause detections (Chu et al. 2019) in comparison with a subset of undisturbed MaRS observations (altitude where the smoothed MaRS electron density is equal to $1 \cdot 10^9 \text{ m}^{-3}$, independent of the presence of a gradient) in dependence of (a) SZA and (b) SZA calibrated solar wind dynamic pressure (Peter et al. 2019). Solar wind parameters are provided by ASPERA-3 (Ramstad et al. 2015)

between 500 and 700 km and are observed less than 15% of the time (Duru et al. 2020). At Mars the topside ionosphere is typically in a magnetized state and the pressure exerted by the ionosphere is dominated by the magnetic pressure component down to approx. 180 to 200 km altitude (Sánchez-Cano et al. 2020b based on MAVEN and MEX ASPERA-3 data, Chu et al. 2021 based on MARSIS data). When the solar wind dynamic pressure increases, the ionopause altitude decreases to lower altitudes (Fig. 11) where the new pressure balance is achieved (Chu et al. 2021). Those events lead to a more compressed ionospheric topside shape with smaller scale heights in the transport region (similar to Fig. 2b) (Ramírez-Nicolás et al. 2016). Sánchez-Cano et al. (2020a) and Chu et al. (2021) both indicate a lesser probability of ionopause formations above strong crustal magnetic fields due to the magnetic pressure added by the crustal fields to the total ionospheric pressure.

The Venus Express and Mars Express radio science experiments observe similar ionospheric topside shapes at Venus and Mars (Peter et al. 2019), ranging from an undisturbed transport region with exponential decay (Fig. 2a), ionopause-like gradients (Fig. 2c) to a fully compressed transport region (Fig. 2b) (Peter et al. 2008; Withers et al. 2012a; Pätzold et al. 2016). No significant change in the extent of the MaRS dayside electron density profiles was found for increasing SZA or increasing solar flux (Fig. 11a). Variations in the solar wind dynamic pressure, however, significantly affect the vertical extent of the ionosphere

Fig. 12 Scheme showing vertical and oblique reflections obtained by MARSIS-AIS due to the presence of enhanced ionospheric density regions over crustal fields. Figure adopted from Duru et al. (2006)



(Fig. 11b), which is in excellent agreement with MARSIS observations (Chu et al. 2019, 2021; Duru et al. 2020).

5.5 The Role of Crustal Magnetic Fields in Controlling the Ionosphere Structure

The Martian ionospheric topside is strongly controlled by magnetic fields. These fields could be either induced from the solar wind, which typically compress the topside of the ionosphere as seen in Fig. 2b, or intrinsic from beneath the surface of the planet, the so-called crustal fields (Acuña et al. 1999). The effect of crustal fields on the vertical structure of the ionosphere is very diverse and depends on the inclination of the magnetic fields. This was clearly demonstrated by Cartacci et al. (2013) who provided the first thorough characterisation of the TEC behaviour with respect to crustal magnetic fields on the Martian nightside based on 6 years of MARSIS-Subsurface observations, and by Mendillo et al. (2013b) who used the same data-set to analyse its day-to-day variability on the planetary dayside as well as the nightside. MARSIS-AIS regularly observes enhancements in the ionospheric electron density as seen in Fig. 12 on the planetary dayside, which occur as oblique reflections on top of vertical (nadir) reflections in the ionograms (Duru et al. 2006) and are found at locations with strong and nearly vertical crustal magnetic fields. It was suggested that the enhancements may be caused by ionospheric heating due to solar wind particles reaching the base of the ionosphere along open field lines (Nielsen et al. 2007). These density enhancements are very stable structures as demonstrated by Andrews et al. (2014). The approximation of a stratified spherically symmetric ionosphere is therefore not valid over regions with strong crustal magnetic fields.

5.6 Solar Activity

Space weather events can cause large variations in the Sun's UV irradiance and charged particle output on short time scales. The interaction of those events with the Mars plasma system can be different from those at Earth due to the lack of an intrinsic global magnetic field. Simultaneous observations of MEX and MAVEN indicate a fast and dynamic response of the Martian ionosphere to the passage of an interplanetary shock wave (Harada et al. 2017). The high solar wind dynamic pressure and SEPs which hit Mars during a strong interplanetary coronal mass ejection (ICME) caused a large disturbance in the Martian plasma system (Fig. 13). The increased solar wind dynamic pressure compressed the ionospheric plasma to lower altitudes and a substantial and severely disturbed ionosphere was observed well beyond the terminator (Morgan et al. 2014). Sánchez-Cano et al. (2017) indicate that the response of the Mars ionosphere to transient space weather events depends

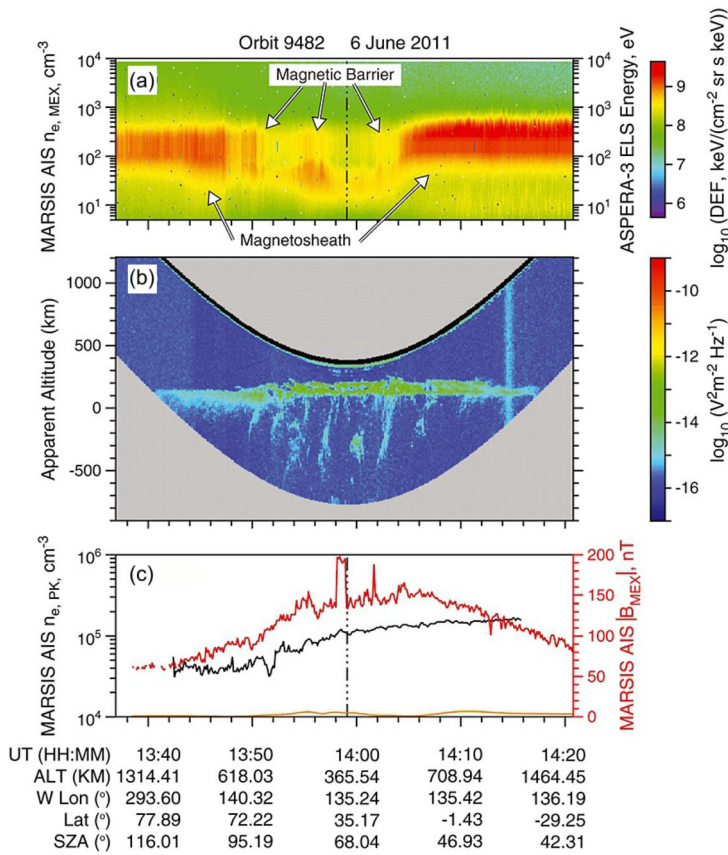


Fig. 13 ASPERA-3 ELS and MARSIS AIS data observed just after an ICME shock hit the Martian ionosphere. The horizontal axis represents time, with corresponding MEX altitude, Mars west longitude, latitude, and SZA. Based on Fig. 5 of Morgan et al. (2014)

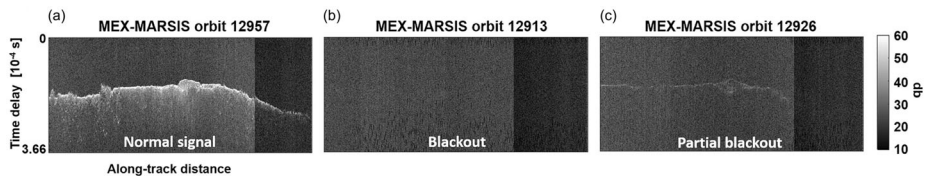


Fig. 14 Radar signals received by MARSIS as a function of time delay. (a) Normal returned MARSIS AIS signal, (b) radar signal during total blackout, (c) partial blackout. Adopted from Fig. 1 of Lester et al. (2022)

on the level of ionization present in the Mars ionosphere, which is based on the solar cycle, Mars’ heliocentric distance and obliquity seasons.

Space weather events can also strongly affect the radio propagation and robotic exploration at Mars. Under normal conditions, the MARSIS radar signal at frequencies higher than the ionospheric peak plasma frequency propagates all the way to the surface of the planet, where it is reflected and eventually propagates back and is detected by the sounder.

However, in some cases the expected surface reflection is partly or totally attenuated for parts of an observation. Such events are due to enhanced ionization at low altitudes which cause increased signal attenuation below the background noise level of the observation (Espley et al. 2007). Němec et al. (2014, 2015) demonstrated that the ground reflections of the MARSIS radar signal on the planetary nightside are almost entirely attenuated during SEP events. The detailed investigation of a 10 day MARSIS radar blackout by Sánchez-Cano et al. (2019) identified SEPs hitting Mars during an extreme space weather event as the source for the extended blackout, implying that space weather events can have significant impact on high frequency communication (e.g. robotic landers/future human exploration) at Mars. This was corroborated by Lester et al. (2022), who investigated the radar blackouts during a full solar cycle (Fig. 14) and found that the blackout events occur on the planetary dayside and nightside with an increased occurrence rate on the nightside and identified a clear correlation with the solar cycle.

5.7 Cometary-Atmospheric Interactions: Flyby of Comet C/2013 A1 (Siding Spring)

Comets and their associated meteor showers are sources of very intense and rapid atmospheric variability that is believed to have strongly affected the evolution of the terrestrial planets in the past. In October 2014, the very close flyby of the Oort-cloud comet C/2013 A1 (Siding-Spring) at only 41.4 Mars radii was a unique opportunity to investigate how a planetary atmosphere behaves in direct contact with the solar wind in combination with a cometary environment. The flyby of Siding-Spring provided the first in-situ observations of cometary energetic particles at Mars (Sánchez-Cano et al. 2018) and MARSIS-AIS observations indicated a very complex and variable ionosphere with rapid density variability, which was stronger than that seen after the impact of large coronal mass ejections. Before closest approach, MARSIS-AIS detected large electron density reductions that seemed to be caused either by comet water damping (the presence of comet water in the ionosphere may lead to a significant rise of hydrogen levels by multiple chemical reactions which may eventually cause a decrease of the local ionospheric electron density) or comet magnetic field interactions, while after the closest approach significant increases in electron density were found (Sánchez-Cano et al. 2020a). A few hours after the flyby, when the cometary dust was well-distributed in the atmosphere, Gurnett et al. (2015) found the first ever detection of a meteoric layer caused by the close encounter of a planet with a comet based on topside sounder observations (Fig. 15). The transient ionized layer was detected at altitudes of about 80 to 100 km with peak electron densities of $(1.5 \text{ to } 2.5) \cdot 10^{11} \text{ m}^{-3}$, which significantly exceeds the electron density values regularly observed in this altitude. The transient layer was sustained for at least 19 h on the nightside and 12 h on the planetary dayside (Venkateswara Rao et al. 2016).

6 Coupling of the Ionosphere with the Lower Atmosphere and Surface

6.1 Ionospheric Seasonal Variability

The eccentricity of the Martian orbit induces a strong seasonal variation in the amount of solar radiation reaching the planet. The main effects on the upper atmosphere are twofold. First, the seasonal variation in the heating of the lower atmosphere induces a contraction/expansion cycle of the atmosphere producing a variation in the atmospheric neutral density at a given altitude. Second, the change in the Sun-Mars distance also directly affects the amount

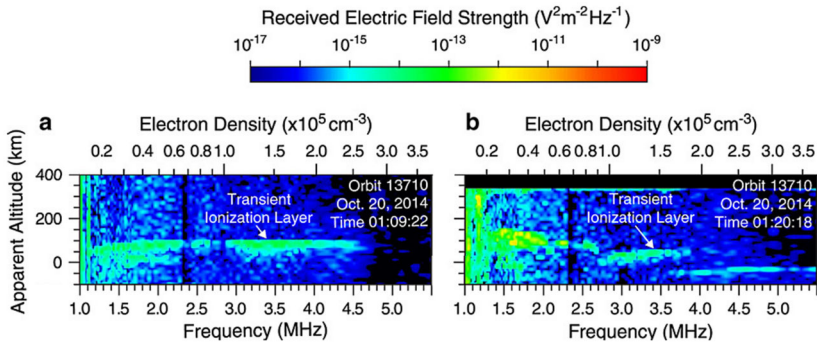


Fig. 15 MARSIS-AIS observations of the transient ionization layer detected at Mars after the transit of comet C/2013 A1 (Siding-Spring) on 19 October 2014. (a) Nightside observations. (b) Dayside observations. Figure adapted from Gurnett et al. (2015)

of ionizing radiation getting to the upper atmosphere. Hints that such variations affected the ionosphere were found by Němec et al. (2011b) who found a correlation between the ionospheric peak altitude derived from MARSIS-AIS data and the Sun-Mars distance, and by Sánchez-Cano et al. (2013) who found a seasonal variation in the MARSIS-AIS ionospheric peak density. A joint analysis of MARSIS-AIS and MaRS data obtained during 15 Earth years confirmed such effects, finding that the seasonal variation of the peak electron density and the peak altitude could be represented by sinusoidal curves with amplitudes around 8–9% and 8–9.5 km, respectively (González-Galindo et al. 2021). It is interesting to note that similar variations are found in the dayglow emissions originated by the absorption of UV solar radiation by CO₂ (see also González-Galindo et al. 2024, this collection).

Other seasonal cycles are induced by the sublimation/condensation of the polar caps. The Martian TEC can be used as a tracer for thermosphere variability, and thanks to the long duration of Mars Express and the good planetary coverage of MARSIS-AIS observations, we can start to unravel the spatial, seasonal, and solar cycle behavior of Mars' ionosphere through the TEC. Figure 16 shows the annual TEC obtained from the MARSIS-Subsurface mode after averaging over all latitudes all available data obtained for SZA=85° during MY 27–32 (Sánchez-Cano et al. 2018). In addition to the expected maximum around perihelion, a second maximum is clearly observed before aphelion that cannot be explained with solar irradiance variability. Instead, it coincides with an increase in the upper atmosphere density of light species. Interesting to note that while the full column of electrons (TEC) has clear indications of this coupling effect, we do not know in which altitude they occur. Observations of the ionospheric peak density (M2 layer) do not display any significant increase at this season, which indicates that this increase should occur at either higher or lower ionospheric regions in the vertical column of the ionosphere (González-Galindo et al. 2021).

6.2 Effects of Atmospheric Dust on the Ionosphere

Dust aerosols are an effective driver for the variability of the Mars neutral atmosphere, which in turn affects the ionosphere by coupling processes with the lower atmosphere. The increase in insolation from Mars aphelion to perihelion in combination with Mars' dust cycle causes a rise of the whole photochemical region of the dayside ionosphere. At times without a global dust storm the average rise is 13 km at the ionospheric base and 22 km closely above the main peak (see Fig. 4, and Peter et al. 2023). Girazian et al. (2020) found a typical peak

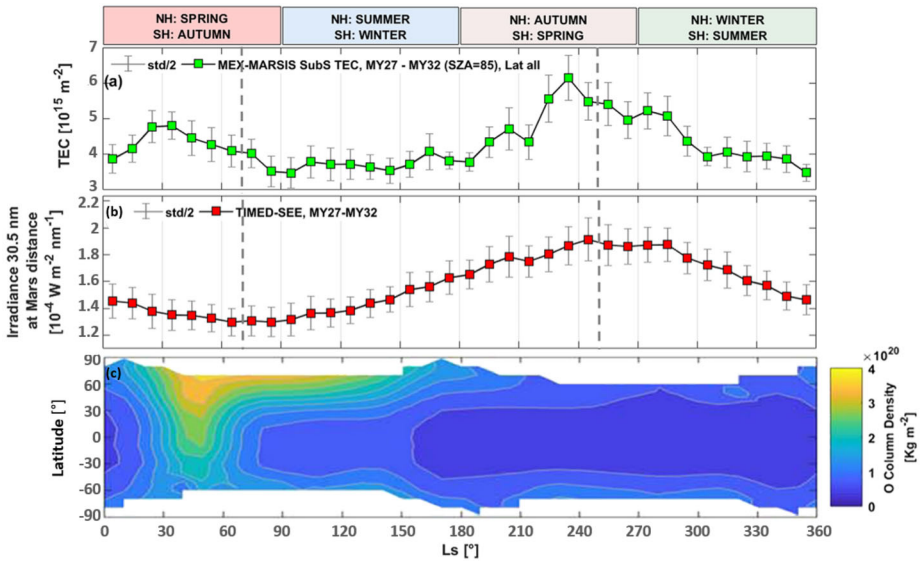


Fig. 16 (a) Annual observations of MEX MARSIS-Subsurface TEC of Martian Years (MY) 27–32 averaged over all latitudes and for SZA = 85°. (b) TIMED-SEE solar irradiance of the 30.5 nm wavelength at Mars' distance (MY 27–32). (c) Ionospheric simulation with the IRAP plasmasphere-ionosphere model (IPIM) model coupled to the Mars Climate Data set (MCD) 5.3 version for SZA = 85°, local time 18 h, and a constant solar flux. The simulation shows the column density between 100 and 200 km of atomic oxygen with latitude and solar longitude (proxy for MY). Figure modified from Sánchez-Cano et al. (2018)

altitude increase of $\sim 10\text{--}15$ km during local and also during global dust storms in 13 years of MARSIS observations (Fig. 17a–c) and a significant increase in upper atmospheric variability. The effect of dust storms on the ionospheric main peak was confirmed by González-Galindo et al. (2021) in their global study of the seasonal and geographical variability of the Martian ionosphere. MaRS ionospheric observations during the global dust storm in 2018 (close to Mars perihelion) indicate that the lifting effect of the storm on the ionospheric main peak region exceeded levels seen during years without a global dust storm. A limit for the warming/expansion of the lower neutral atmosphere and the consecutive lifting of the ionosphere during dust events was identified, which is based on the available insolation at Mars. This limit explains why regional and global dust storms can cause a similar lifting of the ionospheric main peak region (Felici et al. 2020; Peter et al. 2023).

While dust aerosols are regularly found in the lower neutral atmosphere, they can be found in ionospheric altitudes under certain circumstances. One event occurred during March–April 2012, when multiple independent amateur observers detected a localized, high-altitude dust “plume” over the Martian dawn terminator, which was attributed to a large ICME encountering the Martian system at this time (Andrews et al. 2016). Gurnett et al. (2010b) used nearly five years of MARSIS measurements to search for impulsive radio signals generated by possible lightning discharges in the Martian dust storms between 275 and 1400 km altitude. Two major dust storms (and many smaller ones) occurred during the investigated time period. Despite a low detection threshold, no anomalous radio signals attributable to lightning were found.

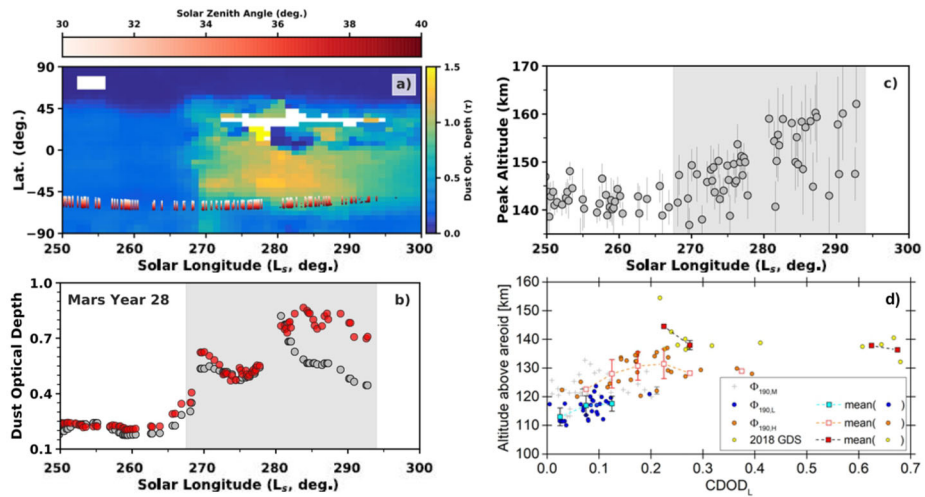


Fig. 17 (a) Zonally averaged column dust optical depth (CDOD) map of the MY28 planet-encircling dust event with MARSIS latitudinal coverage. (b) Globally (gray) and locally (red) averaged CDOD values from individual MARSIS orbits and (c) associated ionospheric peak densities. Gray shaded areas indicate where the peak altitude increases during the dust storm (based on Fig. 5 of Girazian et al. 2020). (d) M2 peak altitudes at $SZA=0^\circ$ derived from MaRS observations in dependence of the local column dust optical depth at 610 Pa ($CDOD_L$) and Φ_{199} solar radiation (based on Fig. 10 of Peter et al. (2023)). The CDOD values are taken from the observation based multi-annual climatology of airborne dust maps of Montabone et al. (2015, 2020)

7 The Contribution of MARSIS and MaRS to the Development of Ionospheric Models

7.1 Empirical Models

The large amount of MARSIS-AIS electron density data obtained over a wide range of SZAs and ionospheric conditions allows the construction of empirical models of the Martian ionospheric electron densities as a function of relevant controlling parameters. Peak electron densities and ionospheric profiles in the photochemically dominated region around the peak altitude are reasonably well described by Chapman-like dependences (Mendillo et al. 2013a, 2018). The capability of such models to predict the peak electron density is demonstrated in Fig. 18a by a direct comparison with peak electron densities determined from the MGS radio occultation measurements. On the other hand, electron densities in the diffusion-dominated region at higher altitudes tend to decrease exponentially (Duru et al. 2008). The corresponding scale height increases with SZA due to the increasing inclination of the induced magnetic field (Němec et al. 2011b), and the respective densities are, to a lesser extent, affected also by crustal magnetic fields (Andrews et al. 2015; Němec et al. 2016) and eventually by the solar cycle (Sánchez-Cano et al. 2015, 2016).

Several empirical formulas were suggested to smoothly connect the altitude dependences in the two regions, allowing the description of electron density profiles above the peak altitude (Němec et al. 2011b, 2019). Although the MARSIS-AIS radar sounding data extend only down to the peak altitude, radio occultation data can be used to study and characterize electron densities at lower altitudes (Sánchez-Cano et al. 2013). Moreover, MARSIS-Subsurface data are used to evaluate and model the Total Electron Content (TEC) (Mendillo et al. 2013b; Bergeot et al. 2019).

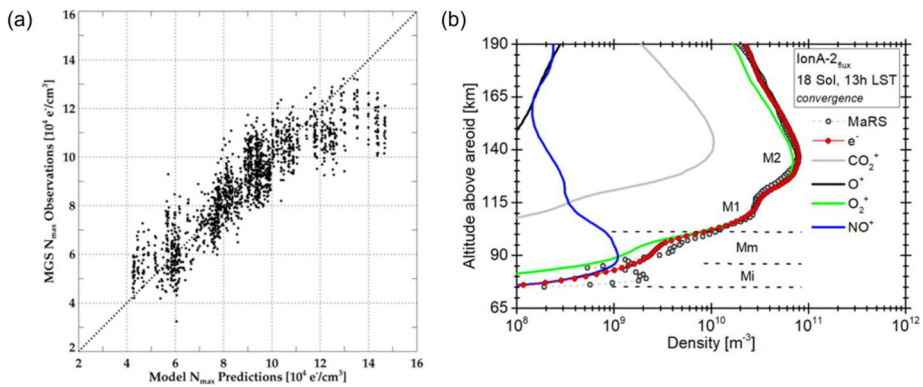


Fig. 18 (a) Comparison of model peak electron densities with MGS observations (adopted from Mendillo et al. 2013a). (b) Comparison between IonA-2 model predictions and a MaRS observation (adopted from Peter et al. 2021)

Ionospheric models based on the MARSIS data have proven to be powerful tools not only to understand the behavior of the ionosphere, but also in several scientific applications, e.g., to support the first ever Mars crosslink radio occultation between two spacecraft (Ao et al. 2015) and the current ESA crosslink tests between MEX and ExoMars-TGO (Nava et al. 2021). Another example is the calculation of the ionospheric phase distortion which is useful to evaluate the effect of the ionosphere on surface clutter detections by the radar sounding (Ilyushin et al. 2017), or new methods for determining the ionospheric TEC (Conroy et al. 2020).

7.2 Photochemical/Transport Models

The unprecedented quality and coverage of MEX ionospheric data has motivated the development of a number of photochemical/transport models and/or has allowed for their validation. In turn, these models have provided a better interpretation of observational results covering most of the topics described in previous sections.

Focusing on the variation of the main ionospheric peaks, the 1D photochemical model of the Boston University was used to analyze quasi-simultaneous radio science observations by MEX and MGS, revealing information about the underlying neutral atmosphere and quantifying the role of secondary ionization in populating the M1 peak (Mendillo et al. 2011). The development of the 1D IonA photochemical model was motivated by MaRS observations of the variability of the main peak, and the comparison between modeled and observed parameters of the M2 peak revealed an overestimation of atmospheric temperatures by the Mars Climate Database (Peter et al. 2014). The presence of a secondary peak in MARSIS TEC during aphelion was attributed to an increased density of light species (such as O) due to the coupling with the lower atmosphere by the coupling of the 1D IRAP plasmasphere-ionosphere model with the Mars Climate Database (Sánchez-Cano et al. 2018). MARSIS peak electron densities obtained at all SZAs enabled validation of the SZA variation predicted by a Global Climate Model incorporating a photochemical ionospheric model, the LMD-MGCM (González-Galindo et al. 2013). A plasma transport module was later incorporated into the LMD-MGCM, which allowed extending its validity to the plasma-dominated region well above the M2 peak. Comparisons with ASPERA-3 trans-terminator velocities showed that

the plasma transport represents a small contribution to the trans-terminator flow at altitudes above about 300 km, with the solar wind being the main driver (Chaufray et al. 2014).

Models have also strongly contributed to our knowledge of the ionosphere below the M1 region. MaRS observations motivated the development of an Indian 1D photochemical model including the interaction of meteoric particles with the Mars atmosphere in order to explore the potential role of meteor ablation in producing some of the observed ionospheric layers in both dayside (Pandya and Haider 2014) and nightside (Haider et al. 2013). The formation mechanisms of excess electron densities below the M1 peak were investigated by comparisons between IonA results and MaRS observations, finding that while some of the observed electron densities can be explained by the penetration of energetic solar radiation, this mechanism can not explain the formation of well defined peaks below the M1 base (Peter et al. 2021) (Fig. 18b).

8 Coordinated Science with Other Instruments and Missions

8.1 MEX Coordination

The Mars Upper Atmosphere Network (MUAN) started in 2009 to improve the Mars Express plasma data coverage and coordination by operating ASPERA-3, MARSIS-AIS and MaRS together in dedicated campaigns for joint data analysis. In order to understand Mars upper atmosphere forcing by the solar wind such campaigns were planned every second year (i.e. in 2010, 2012 and 2014) for a number of weeks, when the instruments were operated in special extended modes. These campaigns were extremely successful and soon started to expand by planning the first coordinated multi-satellite studies of the Mars upper atmosphere by ESA Mars-Express and NASA MAVEN, combining complementary data from various locations in the Mars upper atmosphere and magnetosphere or providing upstream solar wind conditions near Mars for each other. In recent years, this coordination has extended to other missions at Mars. Accomplished science results include:

- The first detailed response (in time and space) of Mars' induced magnetosphere and ionosphere with respect to solar wind variability (Opgenoorth et al. 2013), which could only be done with a dedicated campaign of MARSIS and ASPERA-3.
- A characterisation of the morphology of the topside ionosphere of Mars under different solar wind conditions using ASPERA-3, MARSIS and MaRS (Withers et al. 2016).
- Solar cycle variations of the whole ionosphere due to MaRS and MARSIS-AIS coordination (Sánchez-Cano et al. 2016).
- First evidence of ionospheric forcing being the main driver for the bow shock location, and its seasonal and annual variability based on MARSIS-subsurface TEC and ASPERA-3 magnetosphere observations (Hall et al. 2016, 2019).

8.2 MEX Coordination with Other Missions

The potential of simultaneous observations of individual spacecraft was discovered early in the MEX mission when MEX MARSIS-AIS plasma observations were combined with MGS magnetic field observations to determine conductivities of the dayside ionosphere (Opgenoorth et al. 2010). Same-day ionospheric observations of MGS and MEX radio science provided insights into the temporal and spatial variability of the ionosphere on both hemispheres (Mendillo et al. 2011). Later in the mission, dual spacecraft ionospheric studies

with MAVEN were initiated to study how the Martian ionosphere reacts to the passage of an interplanetary shockwave with upstream plasma and field measurements made by MAVEN and ionospheric observations by MARSIS (Harada et al. 2017), the response of Mars' induced magnetosphere to variations in the upstream solar wind conditions with MARSIS sampling the ionosphere and MAVEN sampling the solar wind (Stergiopoulou et al. 2022), the ionopause formation and pressure balance with MAVEN in the ionosphere and MEX in the solar wind (Sánchez-Cano et al. 2020b) and to characterize the effect of the ionosphere over crustal fields on the bow shock location with MARSIS-subsurface TEC, ASPERA-3 and MAVEN (Garnier et al. 2022b,a). The ionospheric TEC at Earth and Mars has been compared in order to understand the differences and similarities of formation processes under the different magnetic field conditions (Burrell et al. 2020), providing clues on the evolution of Mars' ionosphere from the time when it had a global magnetic field. While the first mutual radio occultation observations at Mars have been conducted between the NASA Odyssey and Mars Reconnaissance Orbiter in 2007 (Ao et al. 2015), they are now regularly conducted between the ExoMars Trace Gas Orbiter and the Mars Express spacecraft since November 2020 (Nava et al. 2021), providing observational coverage independent of Earth occultation seasons and therefore yielding a better temporal and spatial distribution of observations than traditional Earth occultations.

Coordinated science with other instruments and missions was also conducted with MARSIS-AIS and Mars Odyssey High Energy Neutron Detector (HEND) (Morgan et al. 2014), Mars Science Laboratory Radiation Assessment Detector (RAD, for radiation) and the Rover Environmental Monitoring Station (REMS, for atmospheric pressure) (e.g. Sánchez-Cano et al. 2018) and the Mars Reconnaissance Orbiter SHallow RADar (SHARAD) for ionospheric studies (e.g. Campbell and Watters 2016). MARSIS-AIS data have also been proven to be useful for heliospheric studies based on propagation of CMEs and SEPs in the inner heliosphere (Palmerio et al. 2021).

9 Future of Mars Ionosphere Studies

The continuous observation of Mars over the last two decades has led to a significant increase in quantity and variety of information about the thermal structure, composition and variability of the Martian plasma system. It was shown that the ionosphere of Mars is a complex boundary region between the solar wind and the Martian system which is closely and directly coupled with the lower atmosphere and the solar input. Single-spacecraft observations, however, will never be able to provide the whole picture of the Martian plasma dynamics and real-time response to the variability of internal and external drivers (Sánchez-Cano et al. 2021a). The minimum information needed to characterize the response of the ionosphere to the short-time forcing requires at least two observation platforms, which is shown by the successful collaborations between recent and current Mars missions (Sect. 8). However, due to their individually chosen instrumentation and orbit, the scientific possibilities of individually designed spacecraft for combined ionospheric exploration are limited. Coordinated multi-spacecraft missions with high spatial and temporal resolution observations will therefore be the logical path forward in any future robotic / human exploration of Mars. The NASA Mars Orbiters for Surface, Atmosphere, and Ionosphere Connections (MOSAIC) high-level mission concept study (2019-2020) suggests 10 coordinated space-born observation platforms to investigate the drivers of matter and energy flow between and within Mars' diverse climate domains (Lillis et al. 2021a). The Mars Magnetosphere

ATmosphere Ionosphere and Space weather Science (M-MATISSE) mission was successfully submitted to the 2021 ESA M-class call and is currently undergoing the ESA Phase-A study (Sánchez-Cano, the M-MATISSE team 2023). M-MATISSE consists of two spacecraft in coordinated orbits, which shall investigate the global dynamic response of the Martian plasma-atmosphere system to space weather activity. NASA's Escape and Plasma Acceleration and Dynamics Explorers (EscaPADE) mission is scheduled for launch in 2024 and shall unravel the cause-and-effect of solar wind control of ion and sputtering escape by measuring the temporal variability of the upper ionosphere with the two spacecraft passing through the same region a few minutes apart (Lillis et al. 2023). Those missions are the first steps on a road to a deeper understanding of the variability of the Martian ionosphere, the whole planetary climate system and therefore to the successful human exploration of Mars.

Acknowledgements K.P. and M.P. acknowledge support by Bundesministerium für Wirtschaft und Energie, Berlin, via the German Space Agency DLR, Bonn, under grants 50QM1802, and the Deutsche Forschungsgemeinschaft DFG under grants PE3225/2-1 and PA525/25-1. B.S.-C acknowledges support through UK-STFC Ernest Rutherford Fellowship ST/V004115/1, and M.L. through UK-STFC Grant ST/W00089X/1. B.S.-C and M.L. acknowledge support through ESA contract ESA RFP/3-17233/21/ES/JD. F.N. was supported by MSMT Grant LUAUS23152. C.E.R. acknowledges support from STFC studentships ST/S50578X/1 and ST/V507155/1. F.G.-G. acknowledges financial support from the grant CEX2021-001131-S funded by MCIN/AEI/ 10.13039/501100011033.

Declarations

Competing Interests The authors declare no competing interests. F.G.-G. is a Guest Editor of the collection "Mars Express: Pioneering Two Decades of European Science and Exploration of Mars", but has not been involved in the peer review process of this article.

Open Access This article is licensed under a Creative Commons Attribution 4.0 International License, which permits use, sharing, adaptation, distribution and reproduction in any medium or format, as long as you give appropriate credit to the original author(s) and the source, provide a link to the Creative Commons licence, and indicate if changes were made. The images or other third party material in this article are included in the article's Creative Commons licence, unless indicated otherwise in a credit line to the material. If material is not included in the article's Creative Commons licence and your intended use is not permitted by statutory regulation or exceeds the permitted use, you will need to obtain permission directly from the copyright holder. To view a copy of this licence, visit <http://creativecommons.org/licenses/by/4.0/>.

References

- Acuña MH, Connerney JEP, Ness NF et al (1999) Global distribution of crustal magnetization discovered by the Mars Global Surveyor MAG/ER experiment. *Science* 284(5415):790–793. <https://doi.org/10.1126/science.284.5415.790>
- Andrews D, André M, Opgenoorth HJ et al (2014) Oblique reflections in the Mars Express MARSIS data set: stable density structures in the Martian ionosphere. *J Geophys Res Space Phys* 119(5):3944–3960. <https://doi.org/10.1002/2013JA019697>
- Andrews DJ, Edberg NJT, Eriksson AI et al (2015) Control of the topside Martian ionosphere by crustal magnetic fields. *J Geophys Res Space Phys* 120(4):3042–3058. <https://doi.org/10.1002/2014JA020703>
- Andrews DJ, Barabash S, Edberg NJT et al (2016) Plasma observations during the Mars atmospheric "plume" event of March–April 2012. *J Geophys Res Space Phys* 121(4):3139–3154. <https://doi.org/10.1002/2015JA022023>
- Ao CO, Edwards CD Jr, Kahan DS et al (2015) A first demonstration of Mars crosslink occultation measurements. *Radio Sci* 50(10):997–1007. <https://doi.org/10.1002/2015RS005750>
- Barabash S, Lundin R, Andersson H et al (2004) ASPERA-3: analyser of space plasmas and energetic ions for Mars Express. In: Wilson A (ed) *Mars Express*. ESA Publications Division, Noordwijk, pp 121–139.
- Bauer SJ, Hantsch MH (1989) Solar cycle variation of the upper atmosphere temperature of Mars. *Geophys Res Lett* 16(5):373. <https://doi.org/10.1029/GL016i005p00373>

- Bergeot N, Witasse O, Le Maistre S et al (2019) MoMo: a new empirical model of the Mars ionospheric total electron content based on Mars Express MARSIS data. *J Space Weather Space Clim* 9:A36. <https://doi.org/10.1051/swsc/2019035>
- Brace L, Kliore AJ (1991) The structure of the Venus ionosphere. *Space Sci Rev* 55(1–4):81–163. <https://doi.org/10.1007/BF00177136>
- Burrell AG, Sánchez-Cano B, Witasse O et al (2020) Comparison of terrestrial and Martian TEC at dawn and dusk during solstices. *Earth Planets Space* 72(1):790. <https://doi.org/10.1186/s40623-020-01258-3>
- Campbell BA, Watters TR (2016) Phase compensation of MARSIS subsurface sounding data and estimation of ionospheric properties: new insights from SHARAD results. *J Geophys Res, Planets* 121(2):180–193. <https://doi.org/10.1002/2015JE004917>
- Cartacci M, Amata E, Cicchetti A et al (2013) Mars ionosphere total electron content analysis from MARSIS subsurface data. *Icarus* 223(1):423–437. <https://doi.org/10.1016/j.icarus.2012.12.011>
- Chamberlin PC, Eparvier FG, Knoer V et al (2020) The Flare Irradiance Spectral Model—Version 2 (FISM2). *Space Weather* 18(12). <https://doi.org/10.1029/2020SW002588>
- Chaufray JY, González-Galindo F, Forget F et al (2014) Three-dimensional Martian ionosphere model: II. Effect of transport processes due to pressure gradients. *J Geophys Res, Planets* 119(7):1614–1636. <https://doi.org/10.1002/2013JE004551>
- Chicarro A, Martin P, Traunter R (2004) Mars Express: a European mission to the red planet. European Space Agency Publication Division, Noordwijk
- Chu F, Girazian Z, Gurnett DA et al (2019) The effects of crustal magnetic fields and solar EUV flux on ionopause formation at Mars. *Geophys Res Lett* 46(17–18):10257–10266. <https://doi.org/10.1029/2019GL083499>
- Chu F, Girazian Z, Duru F et al (2021) The dayside ionopause of Mars: solar wind interaction, pressure balance, and comparisons with Venus. *J Geophys Res, Planets* E006:936. <https://doi.org/10.1029/2021JE006936>
- Connerney JEP, Acuña MH, Wasilewski PJ et al (2001) The global magnetic field of Mars and implications for crustal evolution. *Geophys Res Lett* 28(21):4015–4018. <https://doi.org/10.1029/2001GL013619>
- Conroy P, Quinsac G, Floury N et al (2020) A new method for determining the total electron content in Mars' ionosphere based on Mars Express MARSIS data. *Planet Space Sci* 104:812. <https://doi.org/10.1016/j.pss.2019.104812>
- Crismani MMJ, Schneider NM, Plane JMC et al (2017) Detection of a persistent meteoric metal layer in the Martian atmosphere. *Nat Geosci* 10:401–404. <https://doi.org/10.1038/ngeo2958>
- Crismani MMJ, Tyo RM, Schneider NM et al (2023) Martian meteoric mg^{+} : atmospheric distribution and variability from maven/iuvs. *J Geophys Res, Planets* E007:315. <https://doi.org/10.1029/2022JE007315>
- Duru F, Gurnett DA, Averkamp TF et al (2006) Magnetically controlled structures in the ionosphere of Mars. *J Geophys Res* 111(A12). <https://doi.org/10.1029/2006JA011975>
- Duru F, Gurnett DA, Morgan DD et al (2008) Electron densities in the upper ionosphere of Mars from the excitation of electron plasma oscillations. *J Geophys Res Space Phys* 113(A7):A07302. <https://doi.org/10.1029/2008JA013073>
- Duru F, Gurnett DA, Frahm RA et al (2009) Steep, transient density gradients in the Martian ionosphere similar to the ionopause at Venus. *J Geophys Res* 114(A12). <https://doi.org/10.1029/2009JA014711>
- Duru F, Baker N, de Boer M et al (2020) Martian ionopause boundary: coincidence with photoelectron boundary and response to internal and external drivers. *J Geophys Res Space Phys* 125(5):121. <https://doi.org/10.1029/2019JA027409>
- Easley JR, Farrell WM, Brain DA et al (2007) Absorption of MARSIS radar signals: solar energetic particles and the daytime ionosphere. *Geophys Res Lett* 23:403. <https://doi.org/10.1029/2006GL028829>
- Felici M, Withers P, Smith MD et al (2020) MAVEN ROSE observations of the response of the Martian ionosphere to dust storms. *J Geophys Res Space Phys* 125(6):26. <https://doi.org/10.1029/2019JA027083>
- Fox JL, Yeager KE (2006) Morphology of the near-terminator Martian ionosphere: a comparison of models and data. *J Geophys Res Space Phys* 111(A10). <https://doi.org/10.1029/2006JA011697>
- Fox JL, Zhou P, Bougher SW (1996) The Martian thermosphere/ionosphere at high and low solar activities. *Adv Space Res* 17(11):203–218. [https://doi.org/10.1016/0273-1177\(95\)00751-Y](https://doi.org/10.1016/0273-1177(95)00751-Y)
- Futaana Y, Barabash S, Yamauchi M et al (2008) Mars Express and Venus express multi-point observations of geoeffective solar flare events in December 2006. *Planet Space Sci* 56(6):873–880. <https://doi.org/10.1016/j.pss.2007.10.014>
- Garnier P, Jacquy C, Gendre X et al (2022a) The drivers of the Martian bow shock location: a statistical analysis of Mars atmosphere and volatile Evolution and Mars Express observations. *J Geophys Res Space Phys* A030:147. <https://doi.org/10.1029/2021JA030147>
- Garnier P, Jacquy C, Gendre X et al (2022b) The influence of crustal magnetic fields on the Martian bow shock location: a statistical analysis of MAVEN and Mars Express observations. *J Geophys Res Space Phys* A030:146. <https://doi.org/10.1029/2021JA030146>

- Girazian Z, Mahaffy P, Lillis RJ et al (2017a) Ion densities in the nightside ionosphere of Mars: effects of electron impact ionization. *Geophys Res Lett* 44(22):11248–11256. <https://doi.org/10.1002/2017GL075431>
- Girazian Z, Mahaffy PR, Lillis RJ et al (2017b) Nightside ionosphere of Mars: composition, vertical structure, and variability. *J Geophys Res Space Phys* 122(4):4712–4725
- Girazian Z, Luppen Z, Morgan DD et al (2020) Variations in the ionospheric peak altitude at Mars in response to dust storms: 13 years of observations from the Mars Express radar sounder. *J Geophys Res, Planets* E006:092. <https://doi.org/10.1029/2019JE006092>
- Girazian Z, Halekas J, Lillis R (2023) Solar cycle and seasonal variability of the nightside ionosphere of Mars: insights from five years of maven observations. *Icarus* 393:114615. <https://doi.org/10.1016/j.icarus.2021.114615>
- González-Galindo F, Chaufray JY, López-Valverde MA et al (2013) Three-dimensional Martian ionosphere model: I. The photochemical ionosphere below 180 km. *J Geophys Res, Planets* 118(10):2105–2123. <https://doi.org/10.1002/jgre.20150>
- González-Galindo F, Eusebio D, Némec F et al (2021) Seasonal and geographical variability of the Martian ionosphere from Mars Express observations. *J Geophys Res, Planets* 126(2):155. <https://doi.org/10.1029/2020JE006661>
- González-Galindo F, Gérard JC, Soret L et al (2024) Airglow and aurora in the Martian atmosphere: contributions by the Mars Express and ExoMars TGO missions. *Space Sci Rev* 220. <https://doi.org/10.1007/s11214-024-01077-y>
- Gurnett DA, Morgan DD, Duru F et al (2010a) Large density fluctuations in the Martian ionosphere as observed by the Mars Express radar sounder. *Icarus* 206(1):83–94. <https://doi.org/10.1016/j.icarus.2009.02.019>
- Gurnett DA, Morgan DD, Granroth LJ et al (2010b) Non-detection of impulsive radio signals from lightning in Martian dust storms using the radar receiver on the Mars Express spacecraft. *Geophys Res Lett* 37(17). <https://doi.org/10.1029/2010GL044368>
- Gurnett DA, Morgan DD, Persoon AM et al (2015) An ionized layer in the upper atmosphere of Mars caused by dust impacts from comet siding spring. *Geophys Res Lett* 42(12):4745–4751. <https://doi.org/10.1002/2015GL063726>
- Haider SA, Pandya BM, Molina-Cuberos GJ (2013) Nighttime ionosphere caused by meteoroid ablation and solar wind electron-proton-hydrogen impact on Mars: MEX observation and modeling. *J Geophys Res Space Phys* 118(10):6786–6794. <https://doi.org/10.1002/jgra.50590>
- Hall BES, Lester M, Sánchez-Cano B et al (2016) Annual variations in the Martian bow shock location as observed by the Mars Express mission. *J Geophys Res Space Phys* 121(11):11474–11494. <https://doi.org/10.1002/2016JA023316>
- Hall BES, Sánchez-Cano B, Wild JA et al (2019) The Martian bow shock over solar cycle 23–24 as observed by the Mars Express mission. *J Geophys Res Space Phys* 124(6):4761–4772. <https://doi.org/10.1029/2018JA026404>
- Harada Y, Gurnett DA, Kopf AJ et al (2017) Dynamic response of the Martian ionosphere to an interplanetary shock: Mars Express and MAVEN observations. *Geophys Res Lett* 44(18):9116–9123. <https://doi.org/10.1002/2017GL074897>
- Harada Y, Gurnett DA, Kopf AJ et al (2018) MARSIS observations of the Martian nightside ionosphere during the September 2017 solar event. *Geophys Res Lett* 45(16):7960–7967. <https://doi.org/10.1002/2018GL077622>
- Ilyushin YA, Orsei R, Witasse O et al (2017) CLUSIM: a synthetic aperture radar clutter simulator for planetary exploration. *Radio Sci* 52(9):1200–1213. <https://doi.org/10.1002/2017RS006265>
- Kahre MA, Murphy JR, Newman CE et al (2017) The Mars dust cycle. In: *The atmosphere and climate of Mars*. Cambridge University Press, Cambridge, pp 295–337. <https://doi.org/10.1017/9781139060172.010>
- Kajdić P, Sánchez-Cano B, Neves-Ribeiro L et al (2021) Interaction of space weather phenomena with Mars plasma environment during solar minimum 23/24. *J Geophys Res Space Phys* A028:442. <https://doi.org/10.1029/2020JA028442>
- Kopf AJ, Gurnett DA, Morgan DD et al (2008) Transient layers in the topside ionosphere of Mars. *Geophys Res Lett* 35(17). <https://doi.org/10.1029/2008GL034948>
- Kopf AJ, Gurnett DA, DiBraccio GA et al (2017) The transient topside layer and associated current sheet in the ionosphere of Mars. *J Geophys Res Space Phys* 122(5):5579–5590. <https://doi.org/10.1002/2016JA023591>
- Lester M, Sanchez-Cano B, Potts D et al (2022) The impact of energetic particles on the Martian ionosphere during a full solar cycle of radar observations: radar blackouts. *J Geophys Res Space Phys* 127(2):3. <https://doi.org/10.1029/2021JA029535>
- Lillis RJ, Brain DA (2013) Nightside electron precipitation at Mars: geographic variability and dependence on solar wind conditions. *J Geophys Res Space Phys* 118(6):3546–3556. <https://doi.org/10.1002/jgra.50171>

- Lillis RJ, Brain DA, England SL et al (2010) Total electron content in the Mars ionosphere: Temporal studies and dependence on solar EUV flux. *J Geophys Res Space Phys* 115(A11). <https://doi.org/10.1029/2010JA015698>
- Lillis RJ, Mitchell DL, Steckiewicz M et al (2018) Ionizing electrons on the Martian nightside: structure and variability. *J Geophys Res Space Phys* 123(5):4349–4363. <https://doi.org/10.1029/2017JA025151>
- Lillis RJ, Mitchell D, Montabone L et al (2021a) MOSAIC: a satellite constellation to enable groundbreaking Mars climate system science and prepare for human exploration. *Planet Sci J* 2(5):211. <https://doi.org/10.3847/PSJ/ac0538>
- Lillis RJ, Xu S, Mitchell D et al (2021b) Ionization efficiency in the dayside ionosphere of Mars: structure and variability. *J Geophys Res, Planets* E006:923. <https://doi.org/10.1029/2021JE006923>
- Lillis RJ, Deighan J, Brain D et al (2022) First synoptic images of fuv discrete aurora and discovery of sinuous aurora at Mars by emm emus. *Geophys Res Lett* L099:820. <https://doi.org/10.1029/2022GL099820>
- Lillis RJ, Curry SM, Curtis D et al (2023) Escapade Update: a Twin-Spacecraft Simplex Mission to Unveil Mars' Unique Hybrid Magnetosphere. Lunar and Planetary Science Conference 2023. Abstract #2806
- Määttänen A, Fedorova MAG, Hernández-Bernal J et al (2024) Dust and clouds on Mars: the view from Mars Express. *Space Sci Rev* 220
- Mayyasi M, Withers P, Fallows K (2018) A sporadic topside layer in the ionosphere of Mars from analysis of MGS radio occultation data. *J Geophys Res Space Phys* 123(1):883–900. <https://doi.org/10.1002/2017JA024938>
- Mendillo M, Lollo A, Withers P et al (2011) Modeling Mars' ionosphere with constraints from same-day observations by Mars Global Surveyor and Mars Express. *J Geophys Res Space Phys* 116(A11). <https://doi.org/10.1029/2011JA016865>
- Mendillo M, Marusiak AG, Withers P et al (2013a) A new semiempirical model of the peak electron density of the Martian ionosphere. *Geophys Res Lett* 40(20):5361–5365. <https://doi.org/10.1002/2013GL057631>
- Mendillo M, Narvaez C, Withers P et al (2013b) Variability in ionospheric total electron content at Mars. *Planet Space Sci* 86(21):117–129. <https://doi.org/10.1016/j.pss.2013.08.010>
- Mendillo M, Narvaez C, Trovato J et al (2018) Mars initial reference ionosphere (MIRI) model: updates and validations using MAVEN, MEX, and MRO data sets. *J Geophys Res Space Phys* 123(7):5674–5683. <https://doi.org/10.1029/2018JA025263>
- Montabone L, Forget F, Millour E et al (2015) Eight-year climatology of dust optical depth on Mars. *Icarus* 251:65–95. <https://doi.org/10.1016/j.icarus.2014.12.034>
- Montabone L, Spiga A, Kass DM et al (2020) Martian year 34 column dust climatology from Mars Climate Sounder observations: reconstructed maps and model simulations. *J Geophys Res, Planets* E006:111. <https://doi.org/10.1029/2019JE006111>
- Morgan DD, Gurnett DA, Kirchner DL et al (2008) Variation of the Martian ionospheric electron density from Mars Express radar soundings. *J Geophys Res* 113(A9). <https://doi.org/10.1029/2008JA013313>
- Morgan DD, Diéval C, Gurnett DA et al (2014) Effects of a strong ICME on the Martian ionosphere as detected by Mars Express and Mars odyssey. *J Geophys Res Space Phys* 119(7):5891–5908. <https://doi.org/10.1002/2013JA019522>
- Mukundan V, Thampi SV, Bhardwaj A (2022) M3 electron density layer in the dayside ionosphere of Mars: analysis of MAVEN ROSE observations. *Icarus* 384(1–4):115062. <https://doi.org/10.1016/j.icarus.2022.115062>
- Nakamura Y, Terada N, Leblanc F et al (2022) Modeling of diffuse auroral emission at Mars: contribution of mev protons. *J Geophys Res Space Phys* A029:914. <https://doi.org/10.1029/2021JA029914>
- Nava B, Migoya-Orue Y, Kashcheyev A et al (2021) Mutual radio occultation experiment between ExoMars Trace Gas Orbiter and Mars Express: algorithms testing. In: European Planetary Science Congress, EPSC2021–605. <https://doi.org/10.5194/epsc2021-605>
- Němec F, Morgan DD, Gurnett DA et al (2010) Nightside ionosphere of Mars: radar soundings by the Mars Express spacecraft. *J Geophys Res* A09:201. <https://doi.org/10.1029/2010JE003663>
- Němec F, Morgan DD, Gurnett DA et al (2011a) Areas of enhanced ionization in the deep nightside ionosphere of Mars. *J Geophys Res, Planets* 116(E6). <https://doi.org/10.1029/2011JE003804>
- Němec F, Morgan DD, Gurnett DA et al (2011b) Dayside ionosphere of Mars: empirical model based on data from the MARSIS instrument. *J Geophys Res* 116(E7):1424. <https://doi.org/10.1029/2010JE003789>
- Němec F, Morgan DD, Diéval C et al (2014) Enhanced ionization of the Martian nightside ionosphere during solar energetic particle events. *Geophys Res Lett* 41(3):793–798. <https://doi.org/10.1002/2013GL058895>
- Němec F, Morgan DD, Diéval C et al (2015) Intensity of nightside MARSIS AIS surface reflections and implications for low–altitude ionospheric densities. *J Geophys Res Space Phys* 120(4):3226–3239. <https://doi.org/10.1002/2014JA020888>
- Němec F, Morgan DD, Gurnett DA et al (2016) Empirical model of the Martian dayside ionosphere: effects of crustal magnetic fields and solar ionizing flux at higher altitudes. *J Geophys Res Space Phys* 121(2):1760–1771. <https://doi.org/10.1002/2015JA022060>

- Němec F, Morgan DD, Kopf AJ et al (2019) Characterizing average electron densities in the Martian dayside upper ionosphere. *J Geophys Res, Planets* 124(1):76–93. <https://doi.org/10.1029/2018JE005849>
- Nielsen E, Fraenz M, Zou H et al (2007) Local plasma processes and enhanced electron densities in the lower ionosphere in magnetic cusp regions on Mars. *Planet Space Sci* 55(14):2164–2172. <https://doi.org/10.1016/j.pss.2007.07.003>
- Opgenoorth HJ, Dhillon RS, Rosenqvist L et al (2010) Day-side ionospheric conductivities at Mars. *Planet Space Sci* 58(10):1139–1151. <https://doi.org/10.1016/j.pss.2010.04.004>
- Opgenoorth HJ, Andrews DJ, Fränz M et al (2013) Mars ionospheric response to solar wind variability. *J Geophys Res Space Phys* 118(10):6558–6587. <https://doi.org/10.1002/jgra.50537>
- Orosei R, Jordan R, Morgan D et al (2015) Mars advanced radar for subsurface and ionospheric sounding (MARSIS) after nine years of operation: a summary. *Planet Space Sci* 112:98–114. <https://doi.org/10.1016/j.pss.2014.07.010>
- Palmerio E, Kilpua EKJ, Witasse O et al (2021) CME magnetic structure and IMF preconditioning affecting SEP transport. *Space Weather* 19(4):e2020SW002. <https://doi.org/10.1029/2020SW002654>
- Pandya BM, Haider SA (2014) Numerical simulation of the effects of meteoroid ablation and solar EUV/X-ray radiation in the dayside ionosphere of Mars: MGS/MEX observations. *J Geophys Res Space Phys* 119:9228–9245. <https://doi.org/10.1002/2014JA020063>
- Pätzold M, Neubauer FM, Carone L et al (2004) MaRS: Mars Express orbiter radio science. In: Wilson A (ed) *Mars Express*. ESA Publications Division, Noordwijk, pp 140–163
- Pätzold M, Tellmann S, Häusler B et al (2005) A sporadic third layer in the ionosphere of Mars. *Science* 310(5749):837–839. <https://doi.org/10.1126/science.1117755>
- Pätzold M, Tellmann S, Andert T et al (2009) MaRS: Mars Express radio science experiment. In: Fletcher K (ed) *Mars Express*. ESA Communication Production Office, Noordwijk, pp 217–245
- Pätzold M, Häusler B, Tyler GL et al (2016) Mars Express 10 years at Mars: observations by the Mars Express radio science experiment (MaRS). *Planet Space Sci* 127:44–90. <https://doi.org/10.1016/j.pss.2016.02.013>
- Peter K (2018) Small scale disturbances in the lower dayside ionosphere of Mars as seen by the radio science experiment MaRS on Mars Express. PhD thesis, Universität zu Köln, Köln. <http://kups.ub.uni-koeln.de/id/eprint/8110>
- Peter K, Pätzold M, Häusler B et al (2008) Ionopause Features of Mars as Observed by the Radio Science Experiment MaRS on Mars Express. American Geophysical Union, Fall Meeting 2008 abstract #P13B-1319
- Peter K, Pätzold M, Molina-Cuberos GJ et al (2014) The dayside ionospheres of Mars and Venus: comparing a one-dimensional photochemical model with MaRS (Mars Express) and VeRa (Venus express) observations. *Icarus* 233:66–82. <https://doi.org/10.1016/j.icarus.2014.01.028>
- Peter K, Chu F, Fränz M et al (2019) Ionopause-like gradients in the ionospheric dayside of Venus and Mars in light of radio science observations. *EPSC-DPS2019-242*
- Peter K, Pätzold M, Molina-Cuberos GJ et al (2021) The lower dayside ionosphere of Mars from 14 years of MaRS radio science observations. *Icarus* 359:114213. <https://doi.org/10.1016/j.icarus.2020.114213>
- Peter K, Pätzold M, Chu F et al (2022) The variability of the topside ionospheres of Venus and Mars in light of radio science observations. <https://doi.org/10.5194/epsc2022-857>
- Peter K, Pätzold M, Montabone L et al (2023) The effects of atmospheric dust and solar radiation on the dayside ionosphere of Mars derived from 17 years of Mars Express radio science observations. *Icarus* 400. <https://doi.org/10.1016/j.icarus.2023.115565>
- Picardi G, Biccari D, Seu R et al (2004) MARSIS: Mars Advanced Radar for Subsurface and Ionosphere Sounding. In: *Mars Express: a European mission to the red planet*. European Space Agency Publication Division, Noordwijk, pp 51–70
- Ramírez-Nicolás M, Sánchez-Cano B, Witasse O et al (2016) The effect of the induced magnetic field on the electron density vertical profile of the Mars' ionosphere: a Mars Express MARSIS radar data analysis and interpretation, a case study. *Planet Space Sci* 126:49–62. <https://doi.org/10.1016/j.pss.2016.03.017>
- Ramstad R, Barabash S, Futaana Y et al (2015) The Martian atmospheric ion escape rate dependence on solar wind and solar EUV conditions: 1. Seven years of Mars Express observations. *J Geophys Res, Planets* 120(7):1298–1309. <https://doi.org/10.1002/2015JE004816>
- Rishbeth H, Mendillo M (2004) Ionospheric layers of Mars and Earth. *Planet Space Sci* 52(9):849–852. <https://doi.org/10.1016/j.pss.2004.02.007>
- Safaieinili A, Kofman W, Mouginot J et al (2007) Estimation of the total electron content of the Martian ionosphere using radar sounder surface echoes. *Geophys Res Lett* 34(23). <https://doi.org/10.1029/2007GL032154>
- Sánchez-Cano B, the M-MATISSE team (2023) The M-MATISSE mission: Mars Magnetosphere ATmosphere Ionosphere and Space weather ScienceE. An ESA Medium class (M7) candidate. EGU General Assembly 2023, Vienna, Austria, 24–28 Apr 2023, EGU23-13687. <https://doi.org/10.5194/egusphere-egu23-13687>

- Sánchez-Cano B, Radicella SM, Herraiz M et al (2013) NeMars: an empirical model of the Martian day-side ionosphere based on Mars Express MARSIS data. *Icarus* 225(1):236–247. <https://doi.org/10.1016/j.icarus.2013.03.021>
- Sánchez-Cano B, Lester M, Witasse O et al (2015) Evidence of scale height variations in the Martian ionosphere over the solar cycle. *J Geophys Res Space Phys* 120(12):10913–10925. <https://doi.org/10.1002/2015JA021949>
- Sánchez-Cano B, Lester M, Witasse O et al (2016) Solar cycle variations in the ionosphere of Mars as seen by multiple Mars Express datasets. *J Geophys Res Space Phys* 121(13):2547–2568. <https://doi.org/10.1002/2015JA022281>
- Sánchez-Cano B, Hall BES, Lester M et al (2017) Mars plasma system response to solar wind disturbances during solar minimum. *J Geophys Res Space Phys* 122(6):6611–6634. <https://doi.org/10.1002/2016JA023587>
- Sánchez-Cano B, Lester M, Witasse O et al (2018) Spatial, seasonal, and solar cycle variations of the Martian total electron content (TEC): is the TEC a good tracer for atmospheric cycles? *J Geophys Res, Planets* 123(7):1746–1759. <https://doi.org/10.1029/2018JE005626>
- Sánchez-Cano B, Witasse O, Lester M et al (2018) Energetic particle showers over Mars from comet C/2013 A1 Siding Spring. *J Geophys Res Space Phys* 123(10):8778–8796. <https://doi.org/10.1029/2018JA025454>
- Sánchez-Cano B, Brelly PL, Lester M et al (2019) Origin of the extended Mars radar blackout of September 2017. *J Geophys Res Space Phys* 124(6):4556–4568. <https://doi.org/10.1029/2018JA026403>
- Sánchez-Cano B, Lester M, Witasse O et al (2020a) Mars' ionospheric interaction with comet C/2013 A1 Siding Spring's coma at their closest approach as seen by Mars Express. *J Geophys Res Space Phys* 125(1):3. <https://doi.org/10.1029/2019JA027344>
- Sánchez-Cano B, Narvaez C, Lester M et al (2020b) Mars' ionopause: a matter of pressures. *J Geophys Res Space Phys* A028:145. <https://doi.org/10.1029/2020JA028145>
- Sánchez-Cano B, Lester M, Andrews DJ et al (2021a) Mars' plasma system. Scientific potential of coordinated multipoint missions: “the next generation”. *Exp Astron* 122:547. <https://doi.org/10.1007/s10686-021-09790-0>
- Sánchez-Cano B, Lester M, Cartacci M et al (2021b) Ionosphere of Mars during the consecutive solar minima 23/24 and 24/25 as seen by MARSIS-Mars Express. *Icarus* 114:616. <https://doi.org/10.1016/j.icarus.2021.114616>
- Steckiewicz M, Garnier P, Lillis R et al (2019) Dawn/dusk asymmetry of the Martian ultraviolet terminator observed through suprathermal electron depletions. *J Geophys Res Space Phys* 124(8):7283–7300. <https://doi.org/10.1029/2018JA026336>
- Stergiopoulou K, Andrews DJ, Edberg NJT et al (2020) Mars Express observations of cold plasma structures in the Martian magnetotail. *J Geophys Res Space Phys* 125(10):51. <https://doi.org/10.1029/2020JA028056>
- Stergiopoulou K, Andrews DJ, Edberg NJT et al (2022) A two-spacecraft study of Mars' induced magnetosphere's response to upstream conditions. *J Geophys Res Space Phys* A030:227. <https://doi.org/10.1029/2021JA030227>
- Thiemann EMB, Chamberlain PC, Eparvier FG et al (2017) The MAVEN EUVM model of solar spectral irradiance variability at Mars: algorithms and results. *J Geophys Res Space Phys* 122(3):2748–2767. <https://doi.org/10.1002/2016JA023512>
- Venkateswara Rao N, ManasaMohana P, Jayaraman A et al (2016) Some new aspects of the transient ionization layer of comet Siding Spring origin in the Martian upper atmosphere. *J Geophys Res Space Phys* 121(4):3592–3602. <https://doi.org/10.1002/2015JA022189>
- Wang H, Richardson MI (2015) The origin, evolution, and trajectory of large dust storms on Mars during Mars years 24–30 (1999–2011). *Icarus* 251:112. <https://doi.org/10.1016/j.icarus.2013.10.033>
- Whalley CL, Plane JMC (2010) Meteoric ion layers in the Martian atmosphere. *Faraday Discuss* 147:349–368. <https://doi.org/10.1039/c003726e>
- Wilson C, Titov D, Holmström M et al (2024) Mars Express scientific payload and its evolution. *Space Sci Rev* 220
- Withers P, Fallows K, Girazian Z et al (2012a) A clear view of the multifaceted dayside ionosphere of Mars. *Geophys Res Lett* 39(18). <https://doi.org/10.1029/2012GL053193>
- Withers P, Fillingim MO, Lillis RJ et al (2012b) Observations of the nightside ionosphere of Mars by the Mars Express Radio Science Experiment (MaRS). *J Geophys Res* 117(A12). <https://doi.org/10.1029/2012JA018185>
- Withers P, Matta M, Lester M et al (2016) The morphology of the topside ionosphere of Mars under different solar wind conditions: results of a multi-instrument observing campaign by Mars Express in 2010. *Planet Space Sci* 120:24–34. <https://doi.org/10.1016/j.pss.2015.10.013>

- Withers P, Felici M, Mendillo M et al (2022) Observations of high densities at low altitudes in the nightside ionosphere of Mars by the MAVEN Radio Occultation Science Experiment (ROSE). *J Geophys Res Space Phys* A030:737. <https://doi.org/10.1029/2022JA030737>
- Xu S, Mitchell D, Liemohn M et al (2017) Martian low-altitude magnetic topology deduced from MAVEN/SWEA observations. *J Geophys Res Space Phys* 122(2):1831–1852. <https://doi.org/10.1002/2016JA023467>

Publisher's Note Springer Nature remains neutral with regard to jurisdictional claims in published maps and institutional affiliations.

Authors and Affiliations

Kerstin Peter¹ · Beatriz Sánchez-Cano²  · František Němec³ · Francisco González-Galindo⁴ · Andrew J. Kopf⁵ · Mark Lester² · Martin Pätzold¹ · Catherine E. Regan⁶ · Mats Holmström⁷

✉ B. Sánchez-Cano
bscmdr1@leicester.ac.uk

K. Peter
Kerstin.Peter@uni-koeln.de

F. Němec
frantisek.nemec@mff.cuni.cz

F. González-Galindo
ggalindo@iaa.es

A.J. Kopf
ajkopf@gmail.com

M. Lester
mle@leicester.ac.uk

M. Pätzold
Martin.Paetzold@uni-koeln.de

C.E. Regan
catherine.regan.19@ucl.ac.uk

M. Holmström
matsh@irf.se

- ¹ Abt. Planetenforschung, Rheinisches Institut für Umweltforschung an der Universität Köln, Cologne, Germany
- ² School of Physics and Astronomy, University of Leicester, Leicester, UK
- ³ Faculty of Mathematics and Physics, Charles University, Prague, Czech Republic
- ⁴ Instituto de Astrofísica de Andalucía, CSIC, Granada, Spain
- ⁵ Celestial Reference Frame Dept., United States Naval Observatory, Washington, DC, USA
- ⁶ Mullard Space Science Laboratory, University College London, London, UK
- ⁷ Swedish Institute of Space Physics, Kiruna, Sweden